Supplementary material for

Contrasting dynamics of hydrological processes in the Volta River basin under global warming

Moctar Dembélé[1,2,7], Mathieu Vrac[3], Natalie Ceperley[7], Sander J. Zwart[1], Josh Larsen[4], Simon J. Dadson[5,6], Grégoire Mariéthoz[2] & Bettina Schaefli[2,7]

[1]International Water Management Institute, CSIR Campus, No. 6 Agostino Neto Road, Accra, Ghana

[2]Institute of Earth Surface Dynamics (IDYST), Faculty of Geosciences and Environment, University of Lausanne, 1015 Lausanne, Switzerland

[3]Laboratoire des Sciences du Climat et de l'Environnement (LSCE-IPSL), CEA/CNRS/UVSQ, Université Paris-Saclay Centre d'Etudes de Saclay, Orme des Merisiers, 91191 Gif-sur-Yvette, France

[4]School of Geography, Earth and Environmental Sciences, University of Birmingham, Birmingham, UK

[5]School of Geography and the Environment, University of Oxford, South Parks Road, Oxford OX1 3QY, UK

[6]UK Centre for Ecology and Hydrology, Wallingford, Oxfordshire OX10 8BB, UK

[7]Institute of Geography (GIUB) and Oeschger Centre for Climate Change Research (OCCR), University of Bern, 3012 Bern, Switzerland

Corresponding author: Moctar Dembélé (moctar.dembele@cgiar.org)

1 Content

This supplementary material file contains additional figures and tables to support the analysis of the results presented in the main manuscript. The methodology used to obtain these results is explained in the main manuscript.

The following sections are presented:

2 Seasonal cycle of hydroclimatic variables

2.1 Rainfall

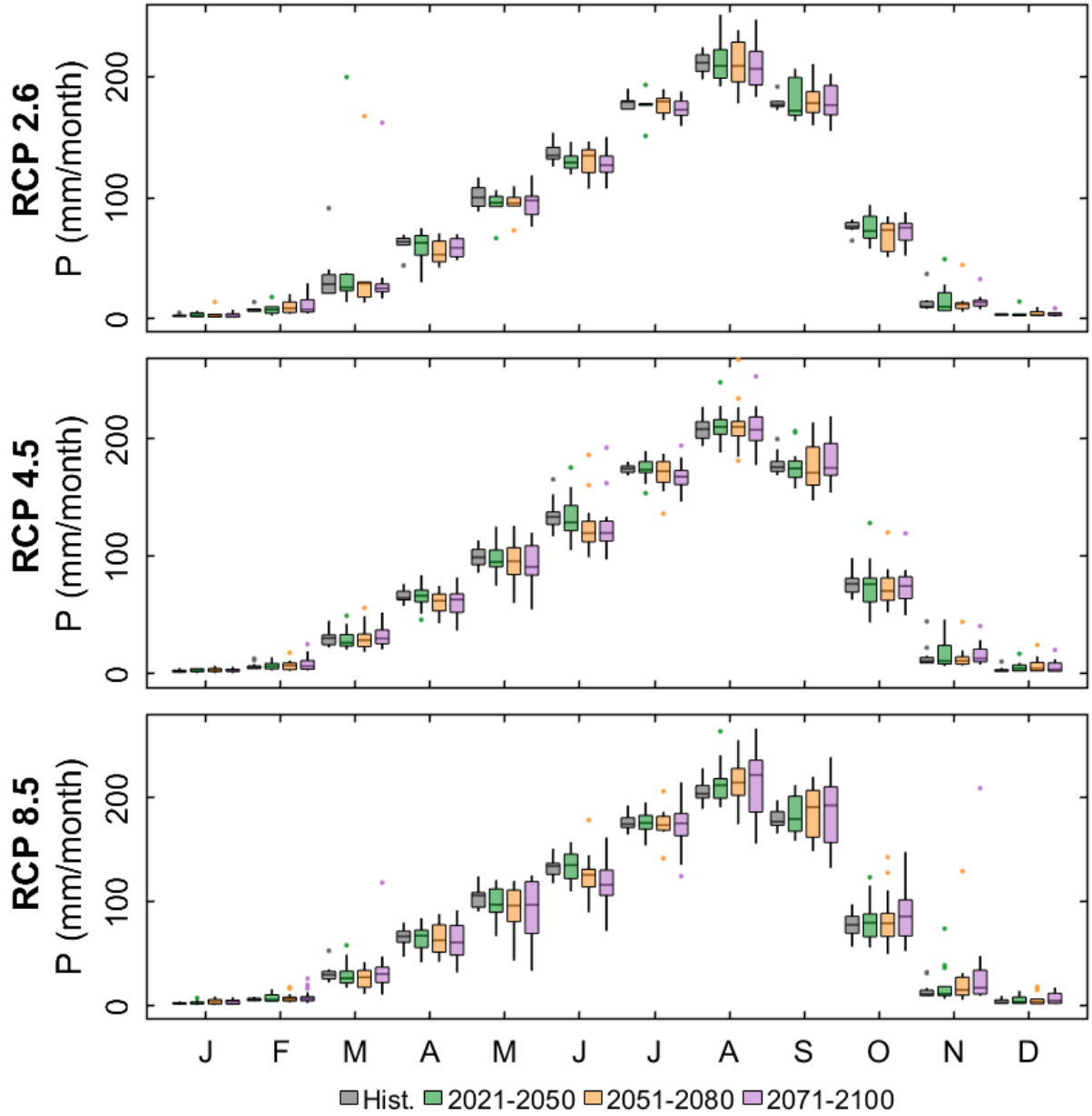

Figure S1. Annual cycles of rainfall (*P*) over the historical and future periods. Each boxplot represents the spread among the RCM-GCMs combinations under RCP2.6 (9 models), RCP4.5 (16 models) and RCP8.5 (18 models).

2.2 Average temperature

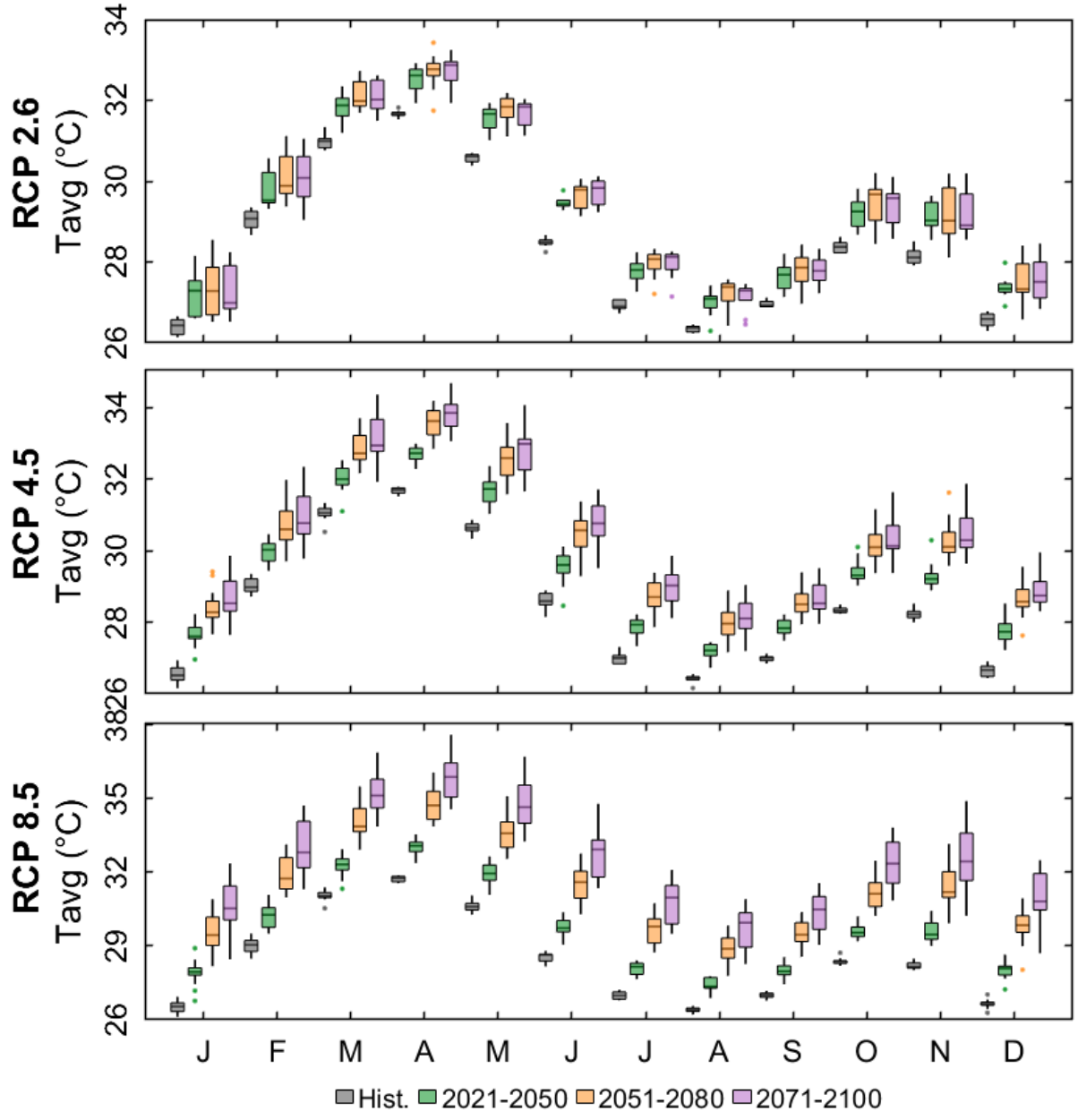

Figure S2. Annual cycles of average air temperature (T_{avg}) over the historical and future periods. Each boxplot represents the spread among the RCM-GCMs combinations under RCP2.6 (9 models), RCP4.5 (16 models) and RCP8.5 (18 models).

2.3 Maximum temperature

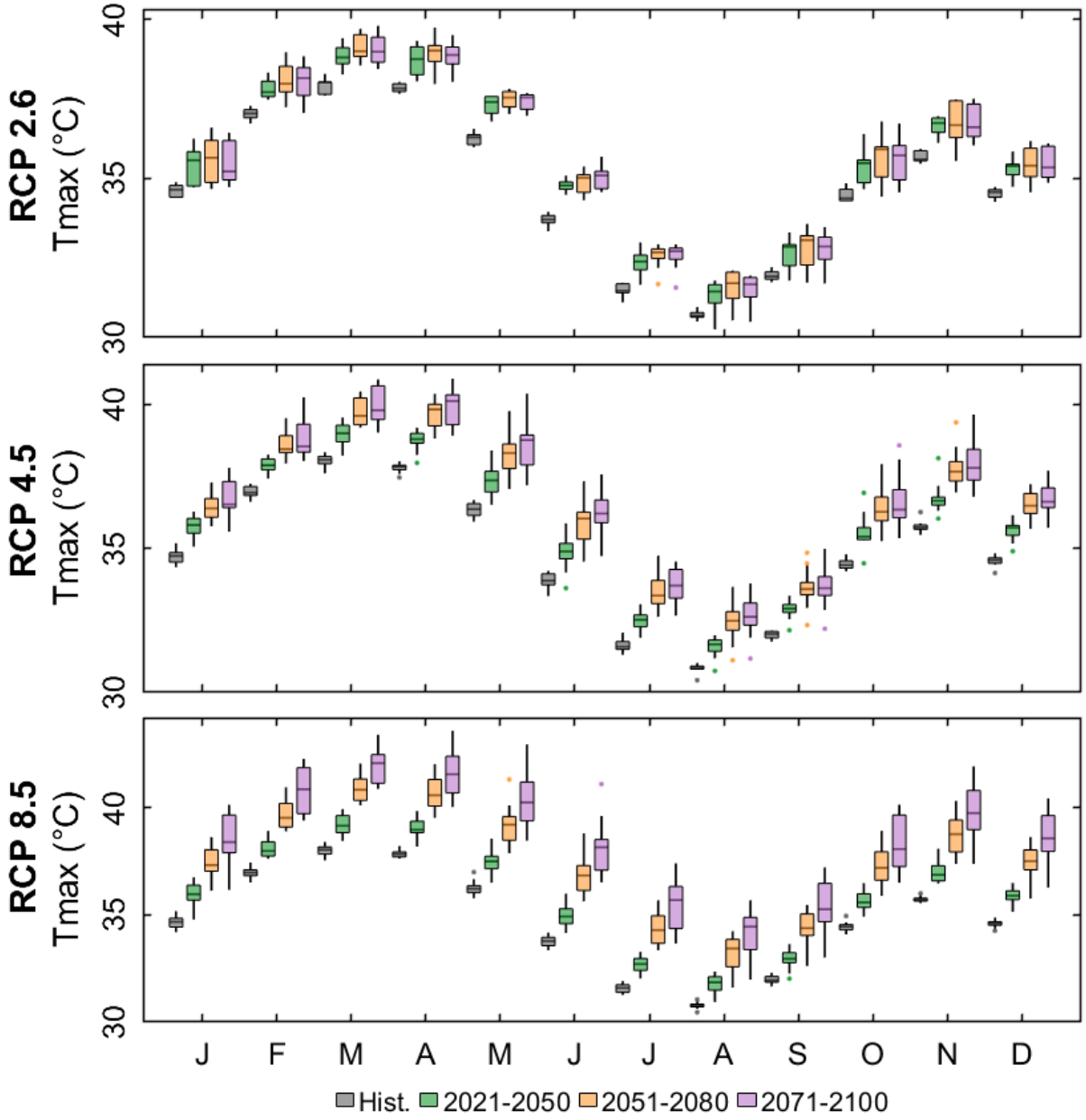

Figure S3. Annual cycles of maximum air temperature (T_{max}) over the historical and future periods. Each boxplot represents the spread among the RCM-GCMs combinations under RCP2.6 (9 models), RCP4.5 (16 models) and RCP8.5 (18 models).

2.4 Minimum temperature

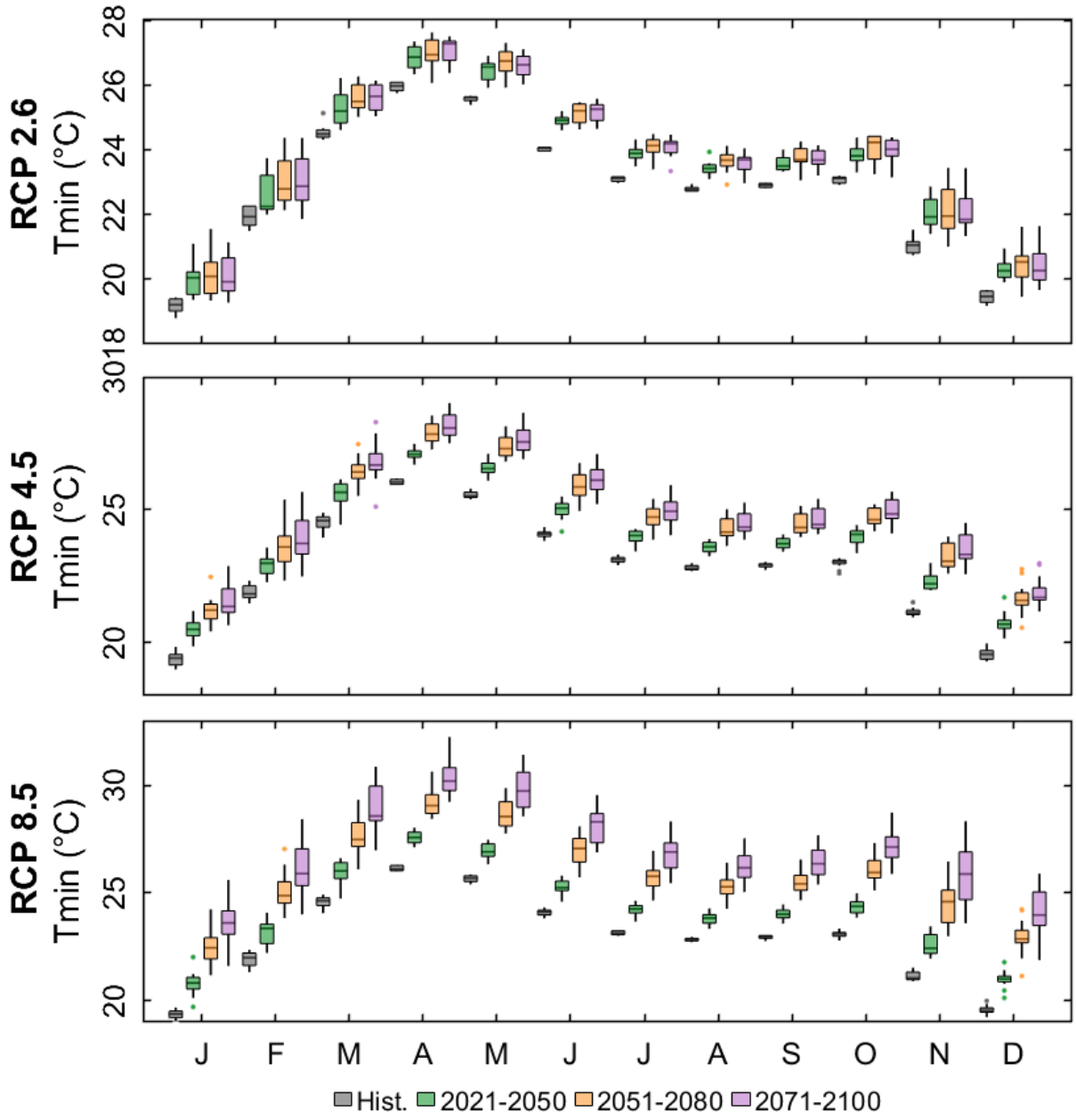

Figure S4. Annual cycles of minimum air temperature (T_{min}) over the historical and future periods. Each boxplot represents the spread among the RCM-GCMs combinations under RCP2.6 (9 models), RCP4.5 (16 models) and RCP8.5 (18 models).

2.5 Potential evaporation

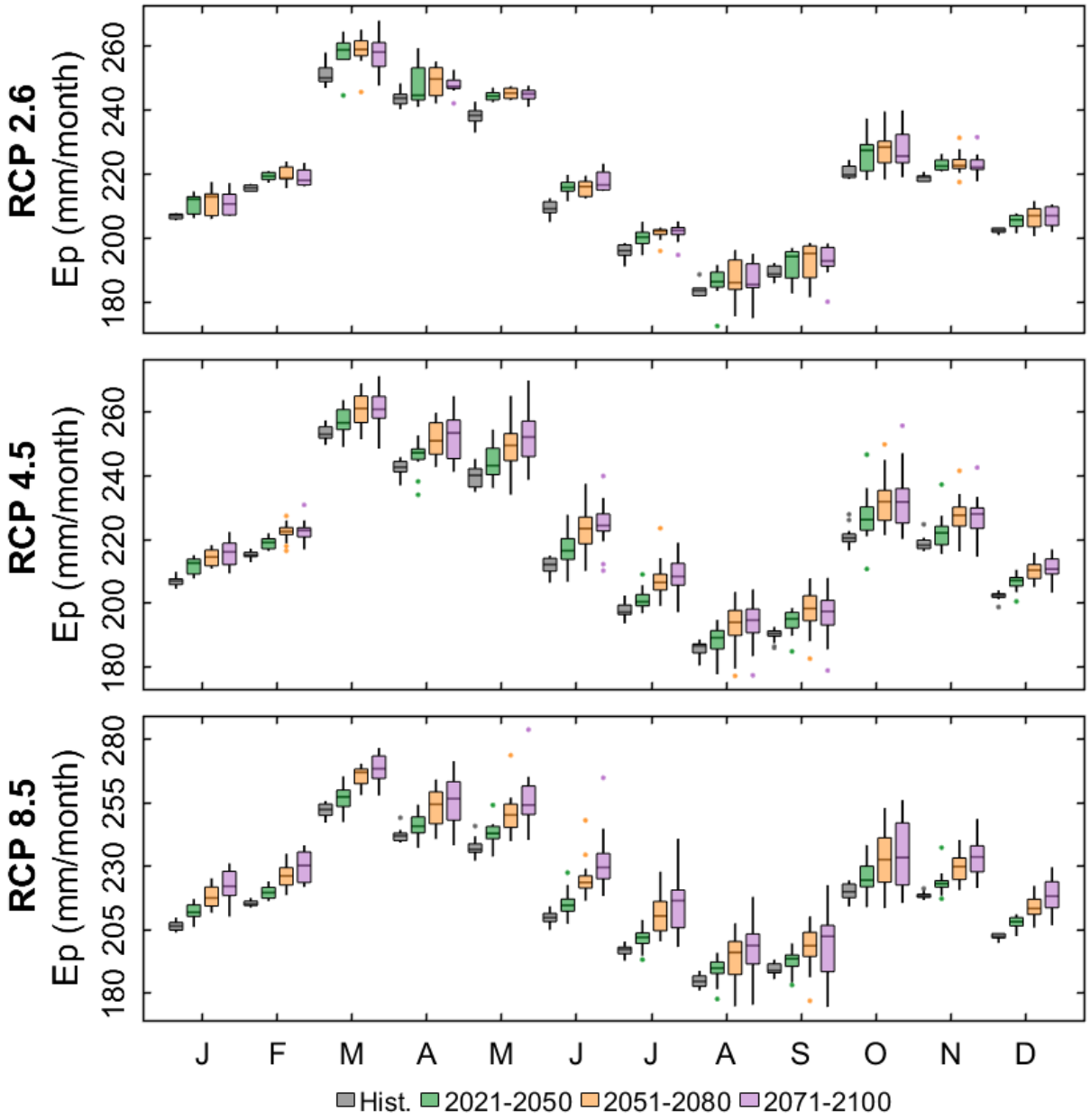

Figure S5. Annual cycles of potential evaporation (*E*p) over the historical and future periods. Each boxplot represents the spread among the RCM-GCMs combinations under RCP2.6 (9 models), RCP4.5 (16 models) and RCP8.5 (18 models).

2.6 Actual evaporation

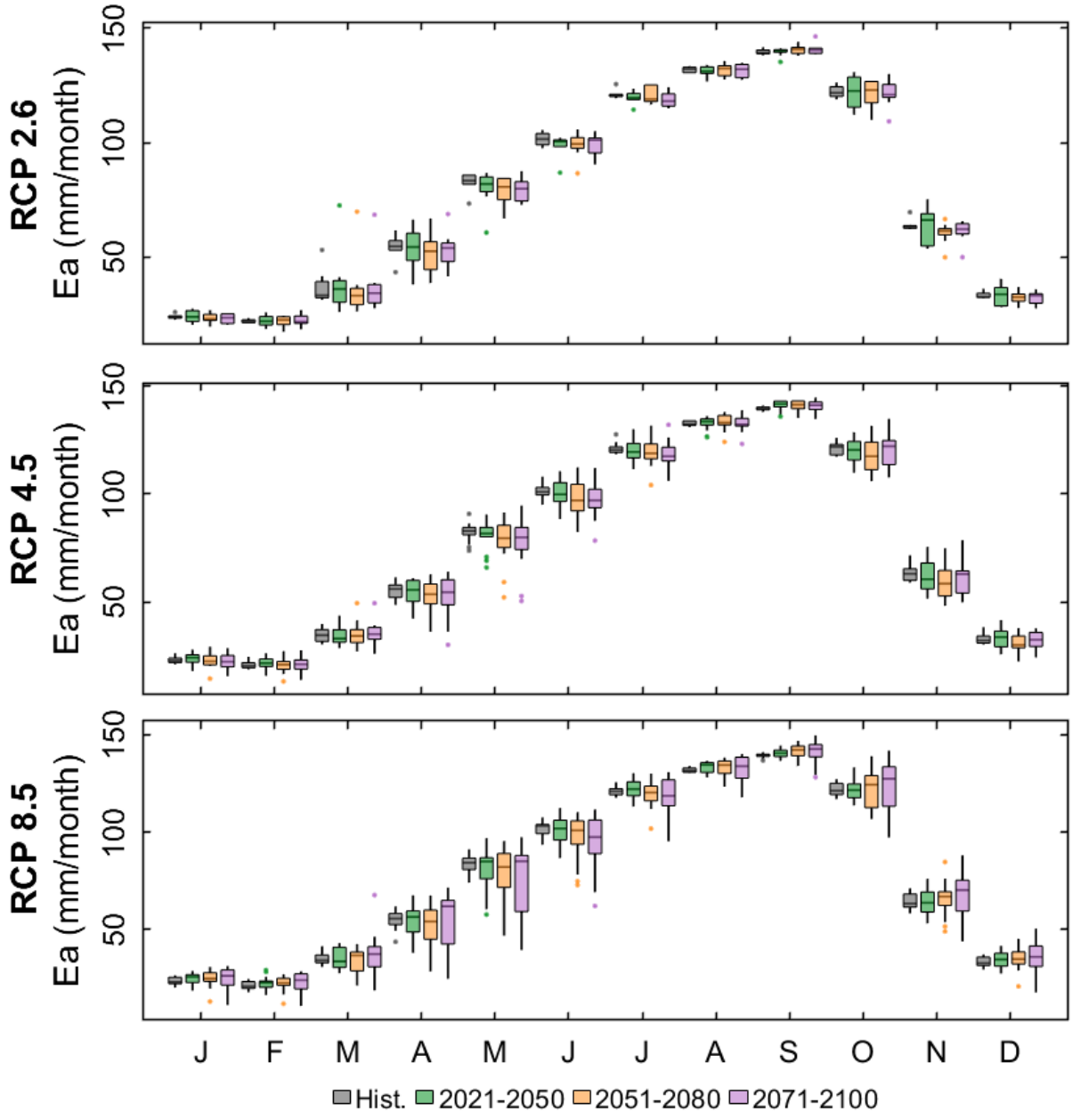

Figure S6. Annual cycles of actual evaporation (*E*a) over the historical and future periods. Each boxplot represents the spread among the RCM-GCMs combinations under RCP2.6 (9 models), RCP4.5 (16 models) and RCP8.5 (18 models).

2.7 Surface runoff

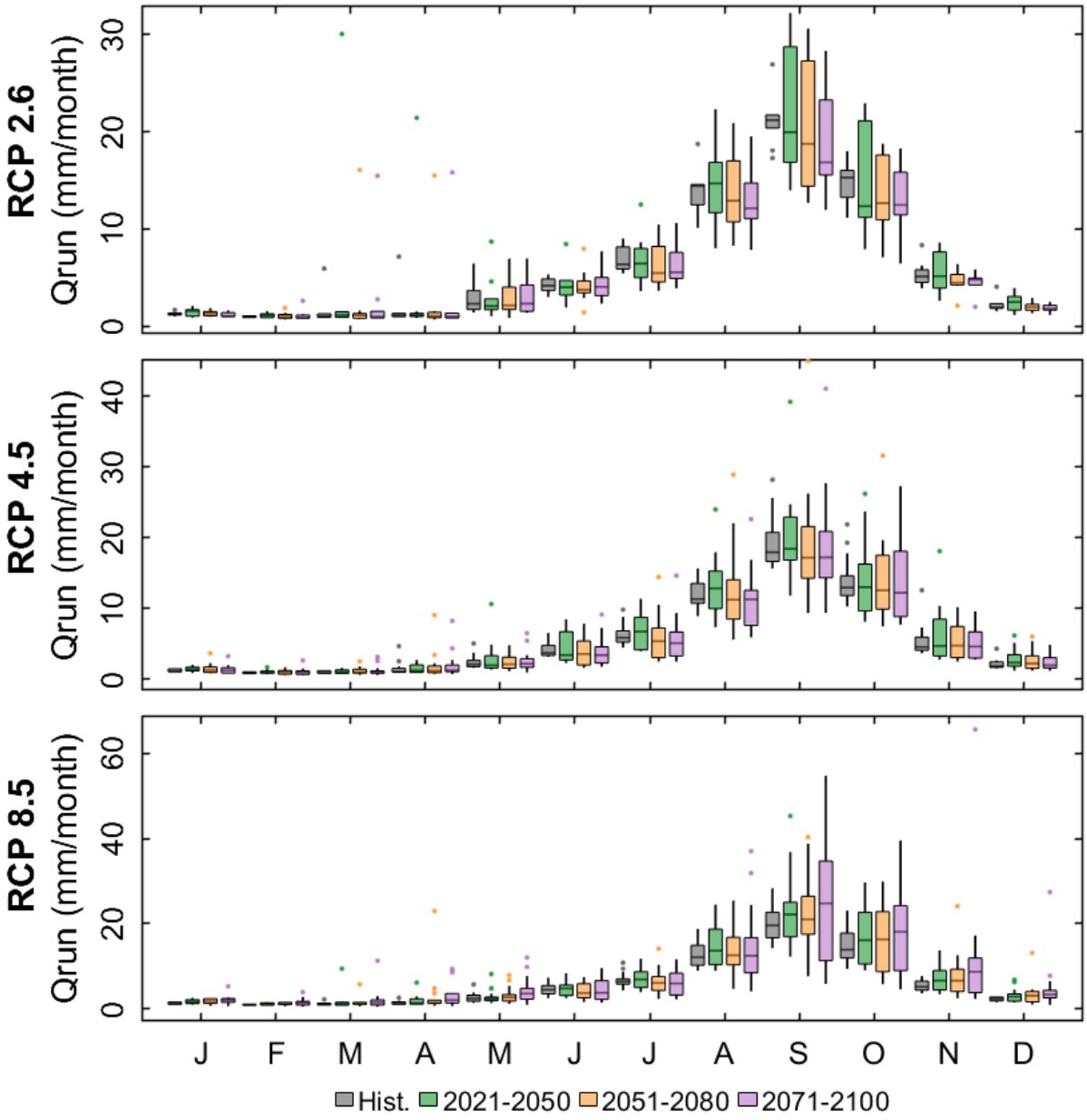

Figure S7. Annual cycles of surface runoff (Q_{run}) over the historical and future periods. Each boxplot represents the spread among the RCM-GCMs combinations under RCP2.6 (9 models), RCP4.5 (16 models) and RCP8.5 (18 models).

2.8 Groundwater recharge

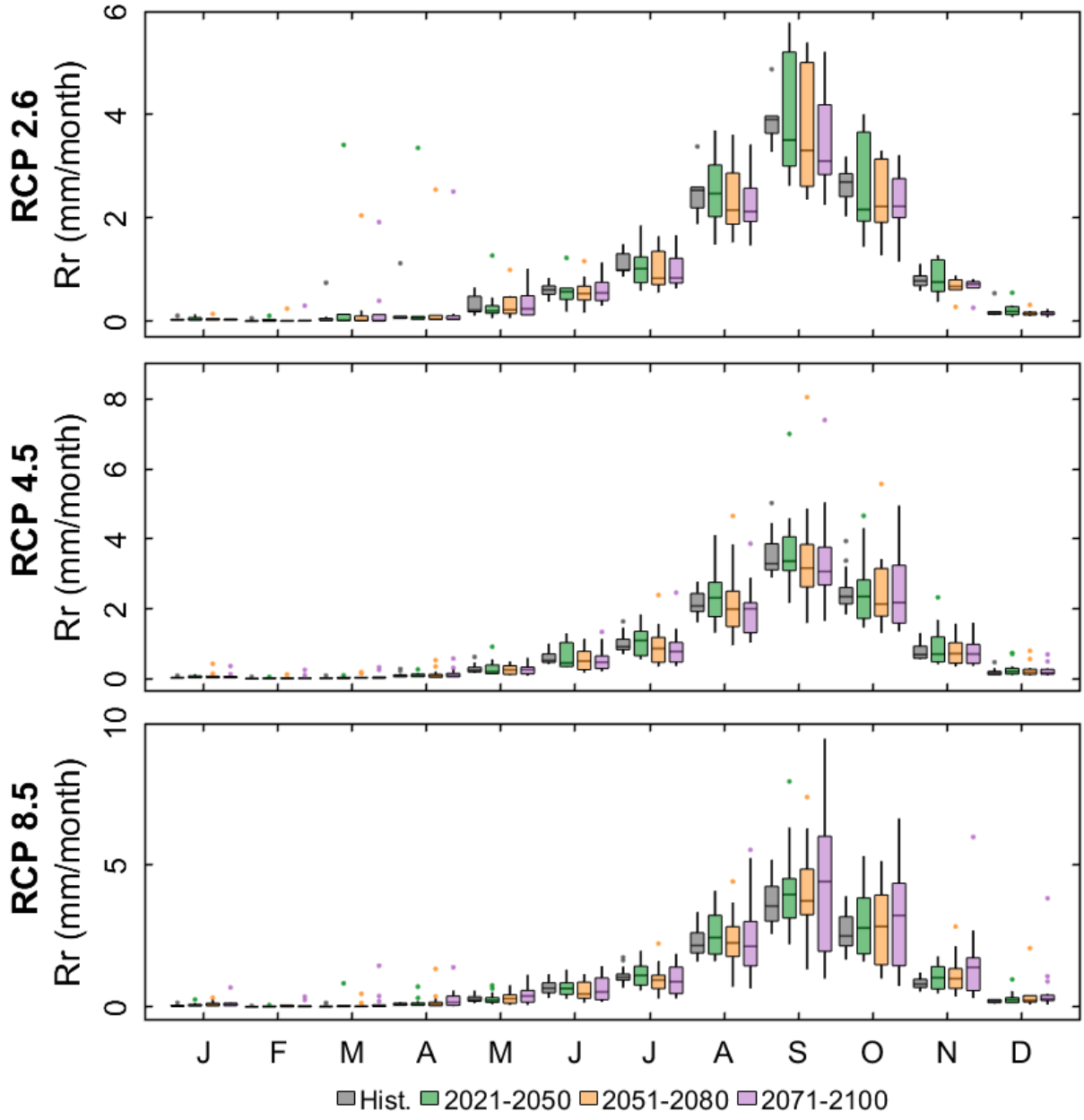

Figure S8. Annual cycles of groundwater recharge (*R*r) over the historical and future periods. Each boxplot represents the spread among the RCM-GCMs combinations under RCP2.6 (9 models), RCP4.5 (16 models) and RCP8.5 (18 models).

2.9 Soil moisture

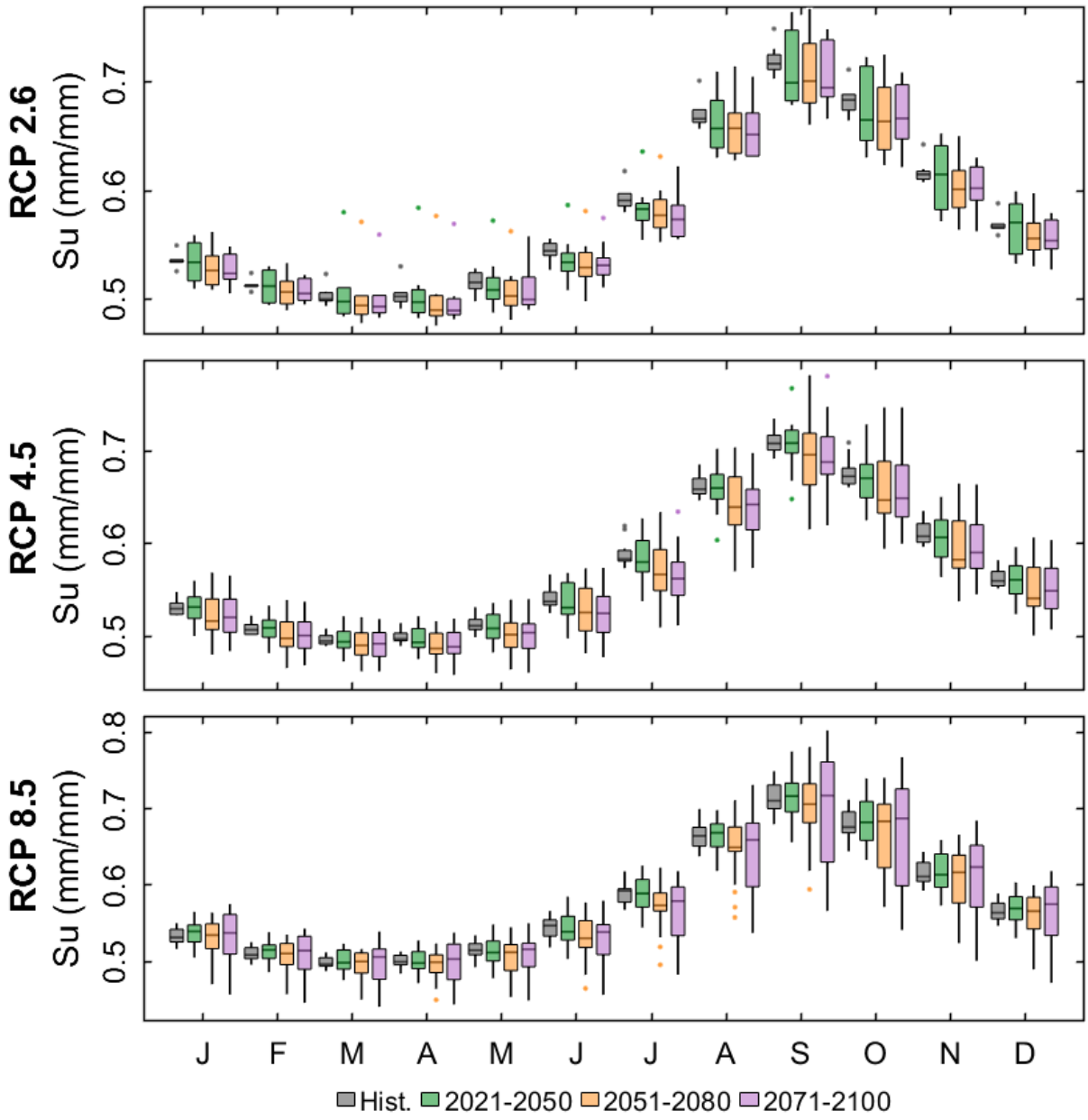

Figure S9. Annual cycles of root-zone soil moisture (*Su*) over the historical and future periods. Each boxplot represents the spread among the RCM-GCMs combinations under RCP2.6 (9 models), RCP4.5 (16 models) and RCP8.5 (18 models).

2.10 Terrestrial water storage

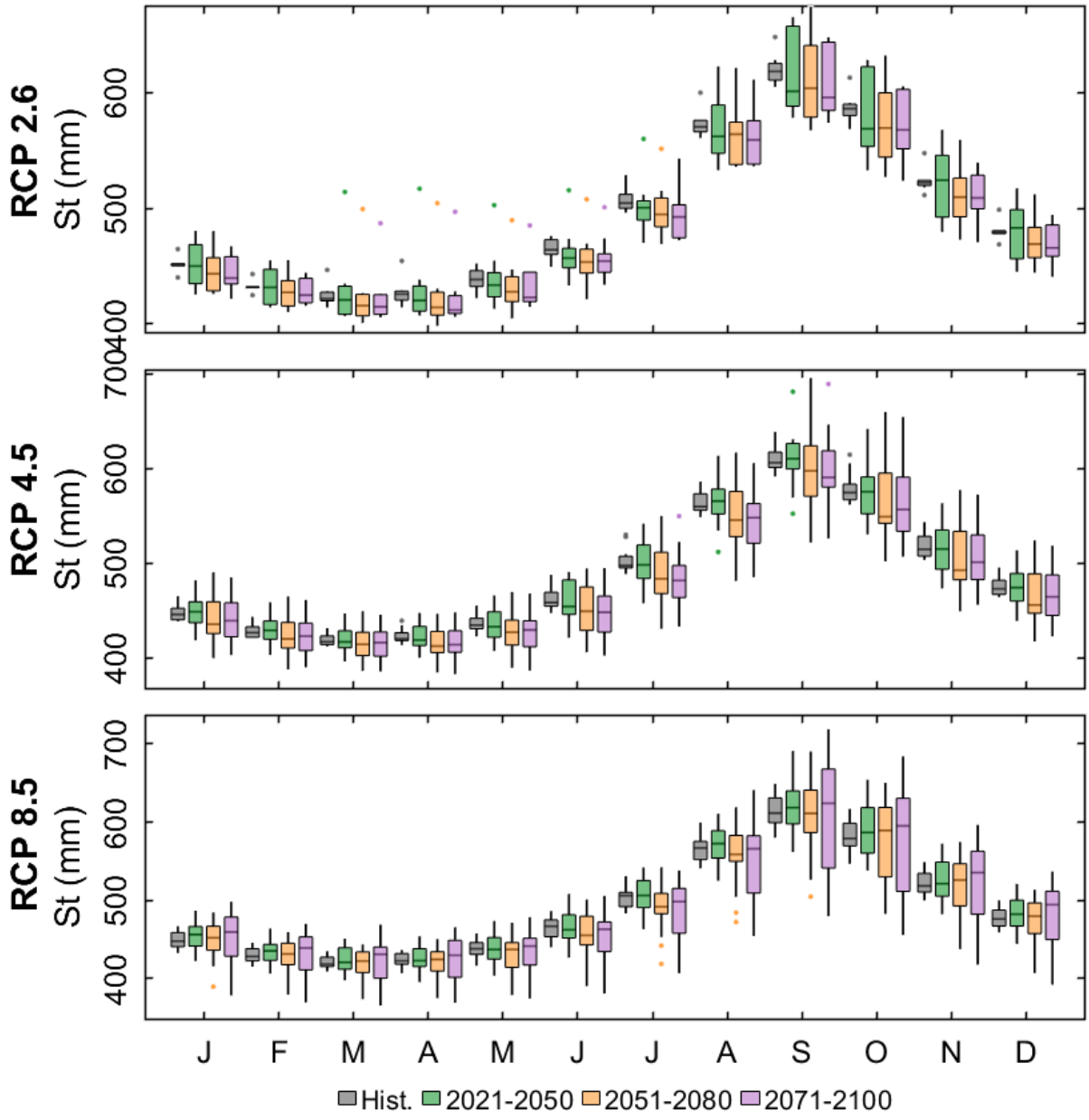

Figure S10. Annual cycles of terrestrial water storage (*St*) over the historical and future periods. Each boxplot represents the spread among the RCM-GCMs combinations under RCP2.6 (9 models), RCP4.5 (16 models) and RCP8.5 (18 models).

3 Changes in the seasonal cycle of hydroclimatic variables

3.1 Rainfall

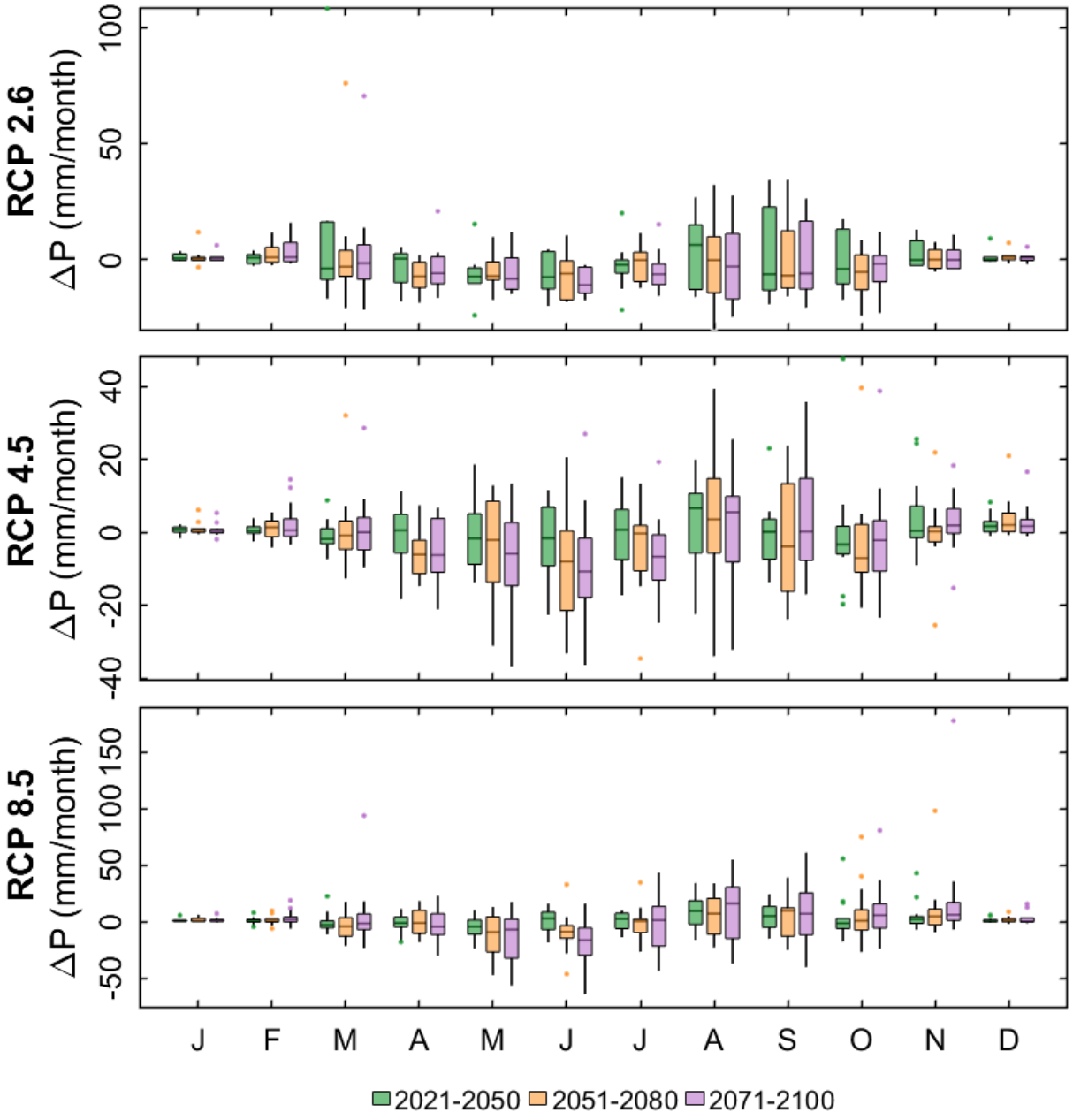

Figure S11. Changes in annual cycles of rainfall (Δ*P*) over the future periods in comparison to the historical period (1991-2020). Each boxplot represents the spread among the RCM-GCMs combinations under RCP2.6 (9 models), RCP4.5 (16 models) and RCP8.5 (18 models).

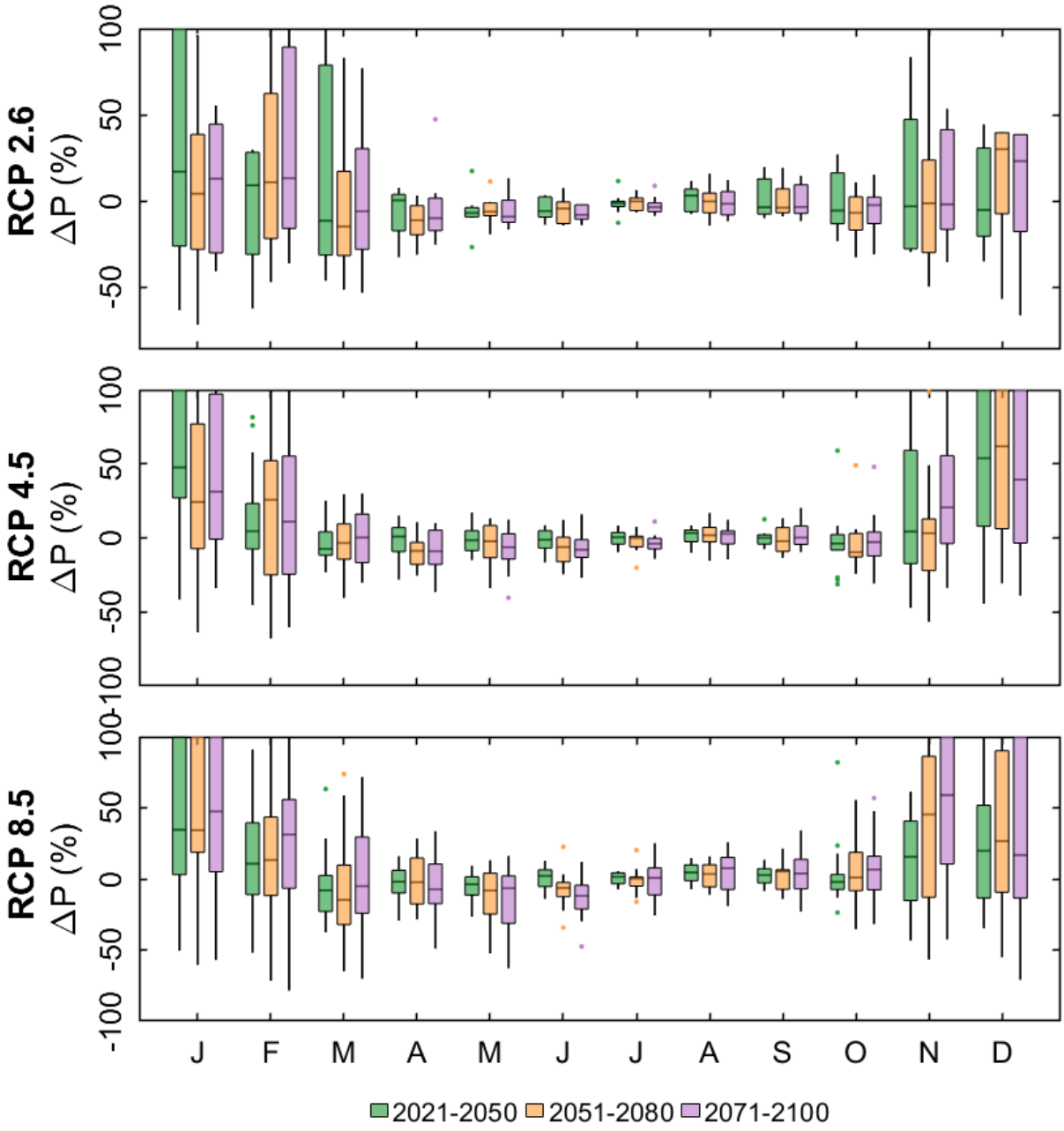

Figure S12. Percentage changes in annual cycles of rainfall (Δ*P*) over the future periods in comparison to the historical period (1991-2020). Each boxplot represents the spread among the RCM-GCMs combinations under RCP2.6 (9 models), RCP4.5 (16 models) and RCP8.5 (18 models).

3.2 Average temperature

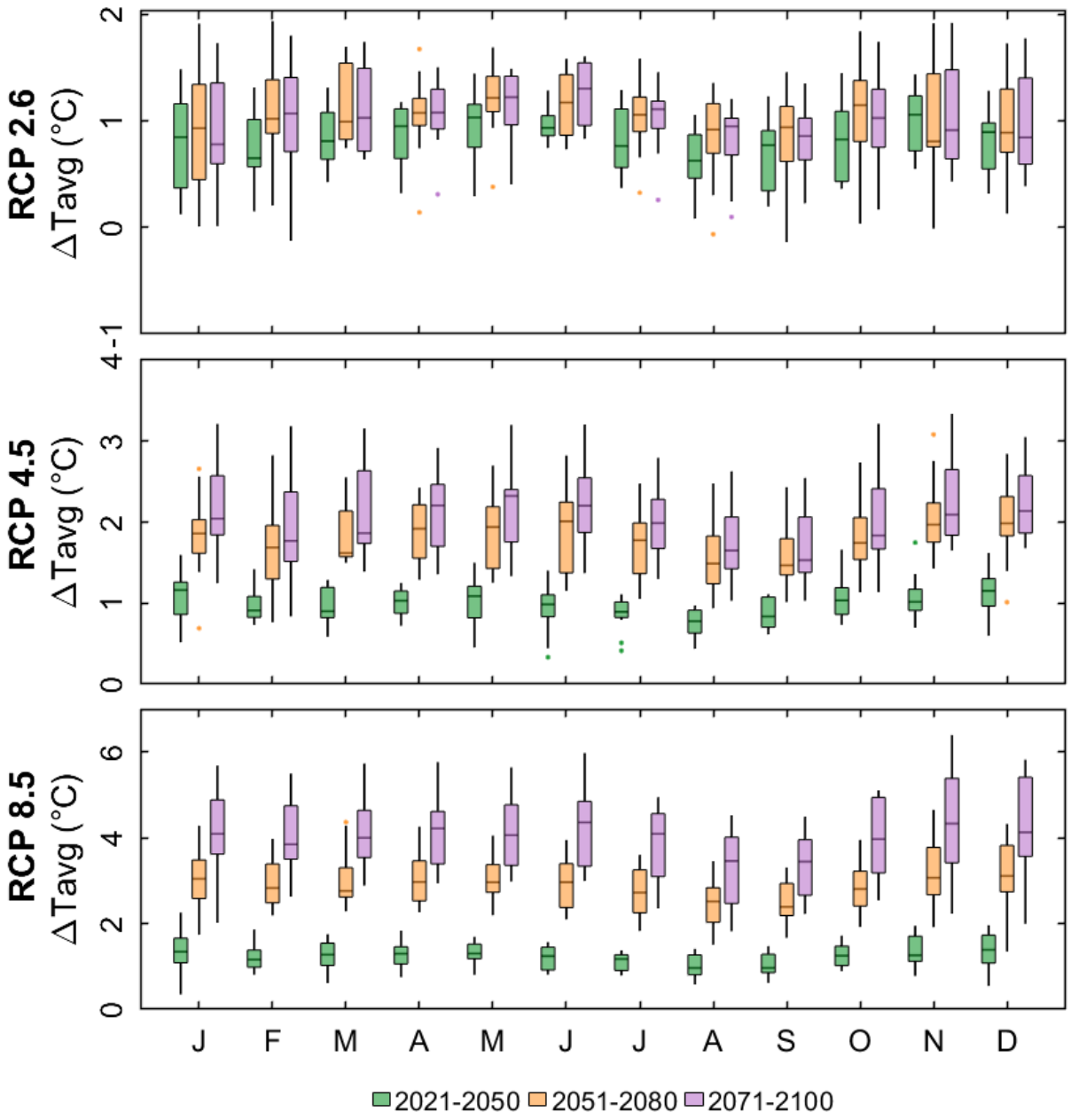

Figure S13. Changes in annual cycles of average air temperature (ΔT_{avg}) over the future periods in comparison to the historical period (1991-2020). Each boxplot represents the spread among the RCM-GCMs combinations under RCP2.6 (9 models), RCP4.5 (16 models) and RCP8.5 (18 models).

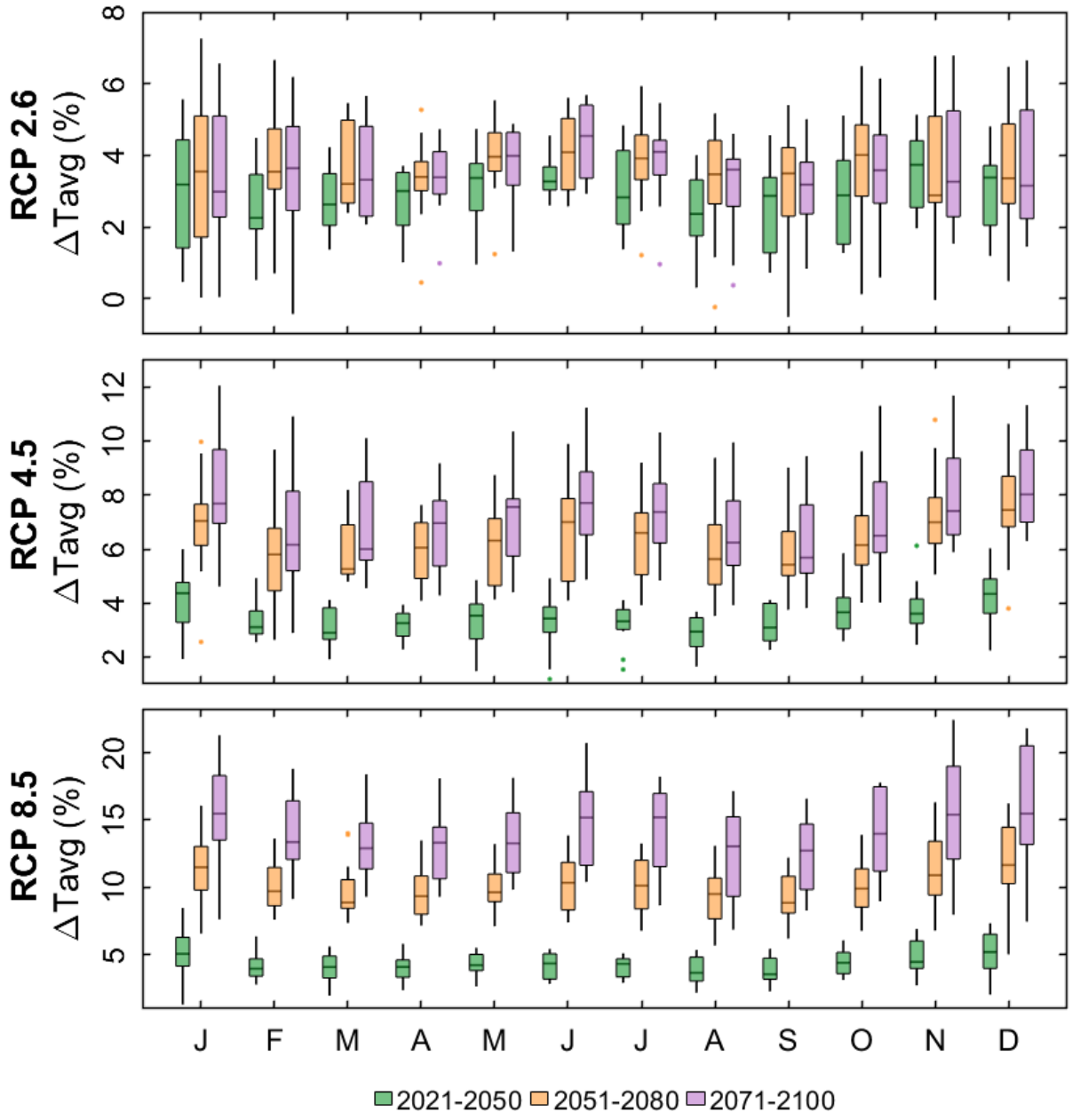

Figure S14. Percentage changes in annual cycles of average air temperature (ΔT_{avg}) over the future periods in comparison to the historical period (1991-2020). Each boxplot represents the spread among the RCM-GCMs combinations under RCP2.6 (9 models), RCP4.5 (16 models) and RCP8.5 (18 models).

3.3 Maximum temperature

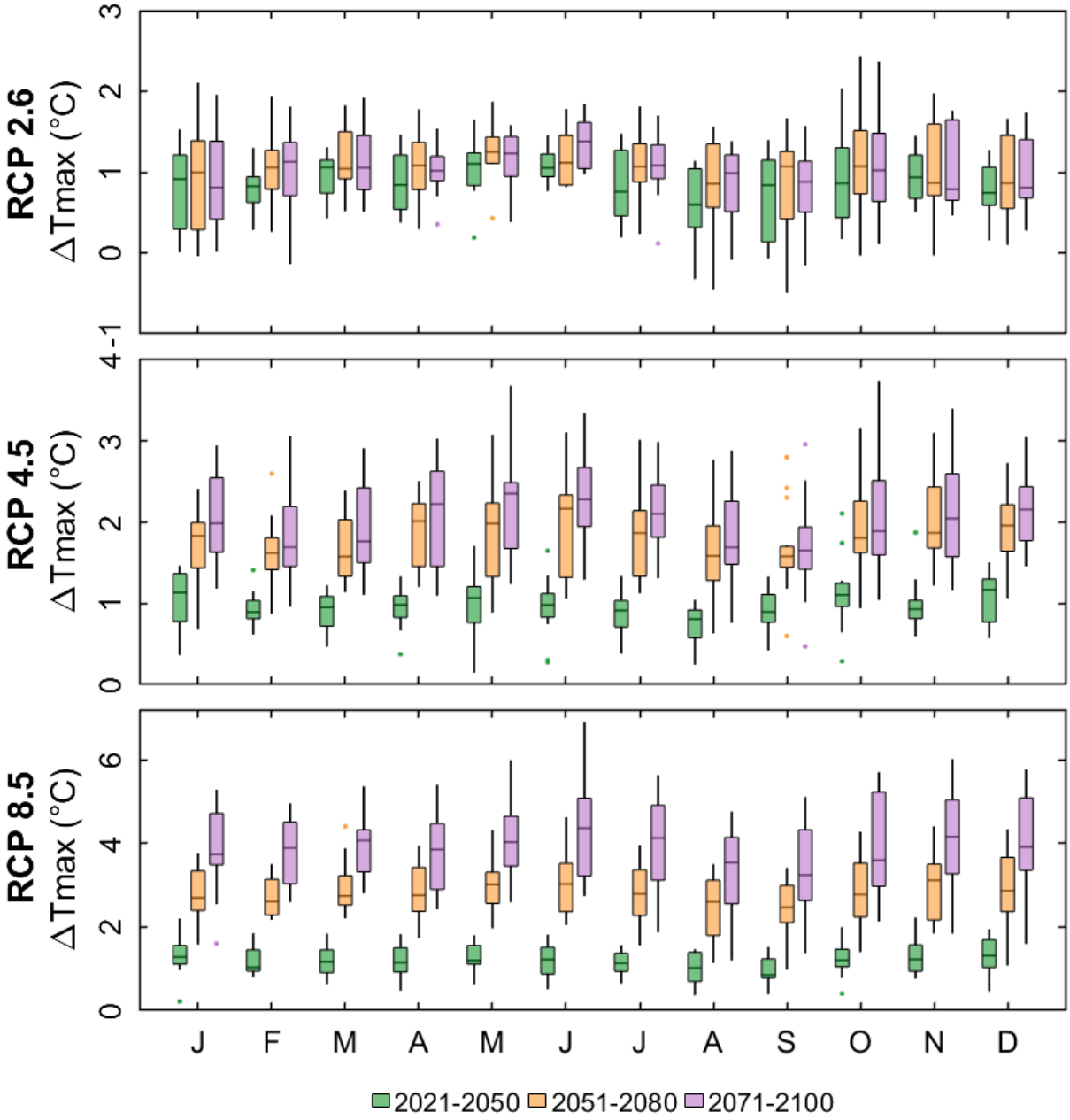

Figure S15. Changes in annual cycles of maximum air temperature (ΔT_{max}) over the future periods in comparison to the historical period (1991-2020). Each boxplot represents the spread among the RCM-GCMs combinations under RCP2.6 (9 models), RCP4.5 (16 models) and RCP8.5 (18 models).

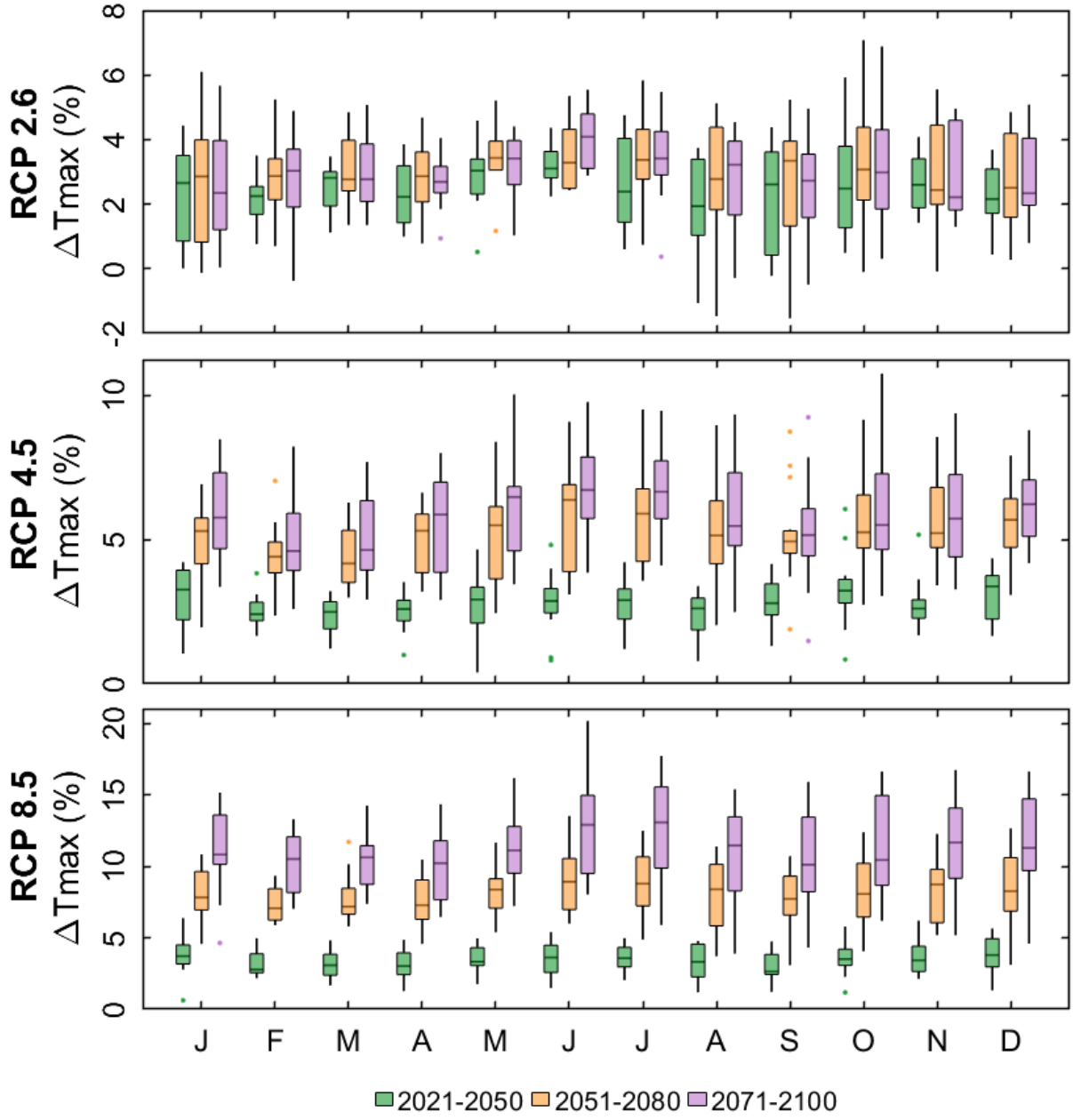

Figure S16. Percentage changes in annual cycles of maximum air temperature (ΔT_{max}) over the future periods in comparison to the historical period (1991-2020). Each boxplot represents the spread among the RCM-GCMs combinations under RCP2.6 (9 models), RCP4.5 (16 models) and RCP8.5 (18 models).

3.4 Minimum temperature

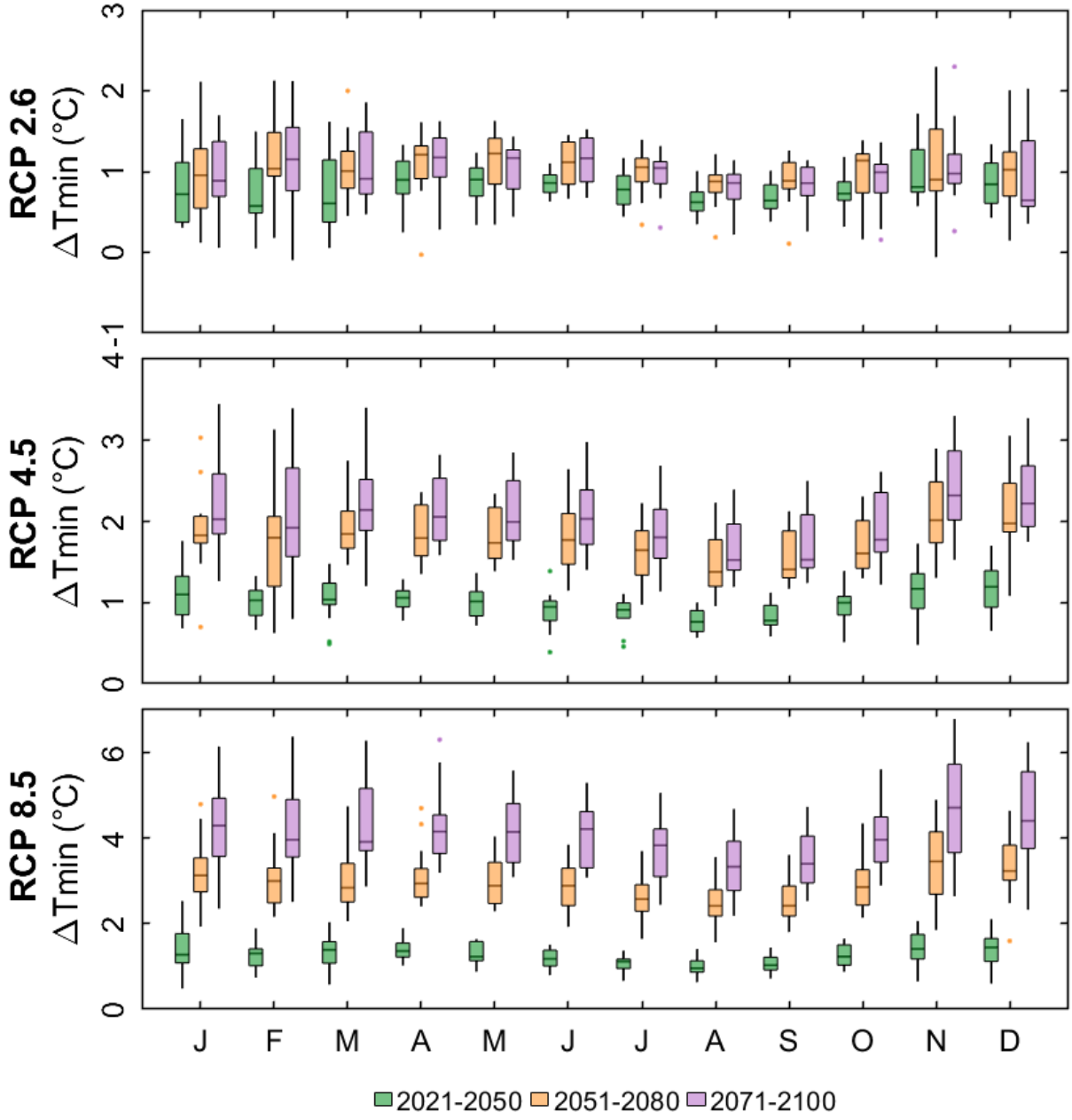

Figure S17. Changes in annual cycles of minimum air temperature (ΔT_{min}) over the future periods in comparison to the historical period (1991-2020). Each boxplot represents the spread among the RCM-GCMs combinations under RCP2.6 (9 models), RCP4.5 (16 models) and RCP8.5 (18 models).

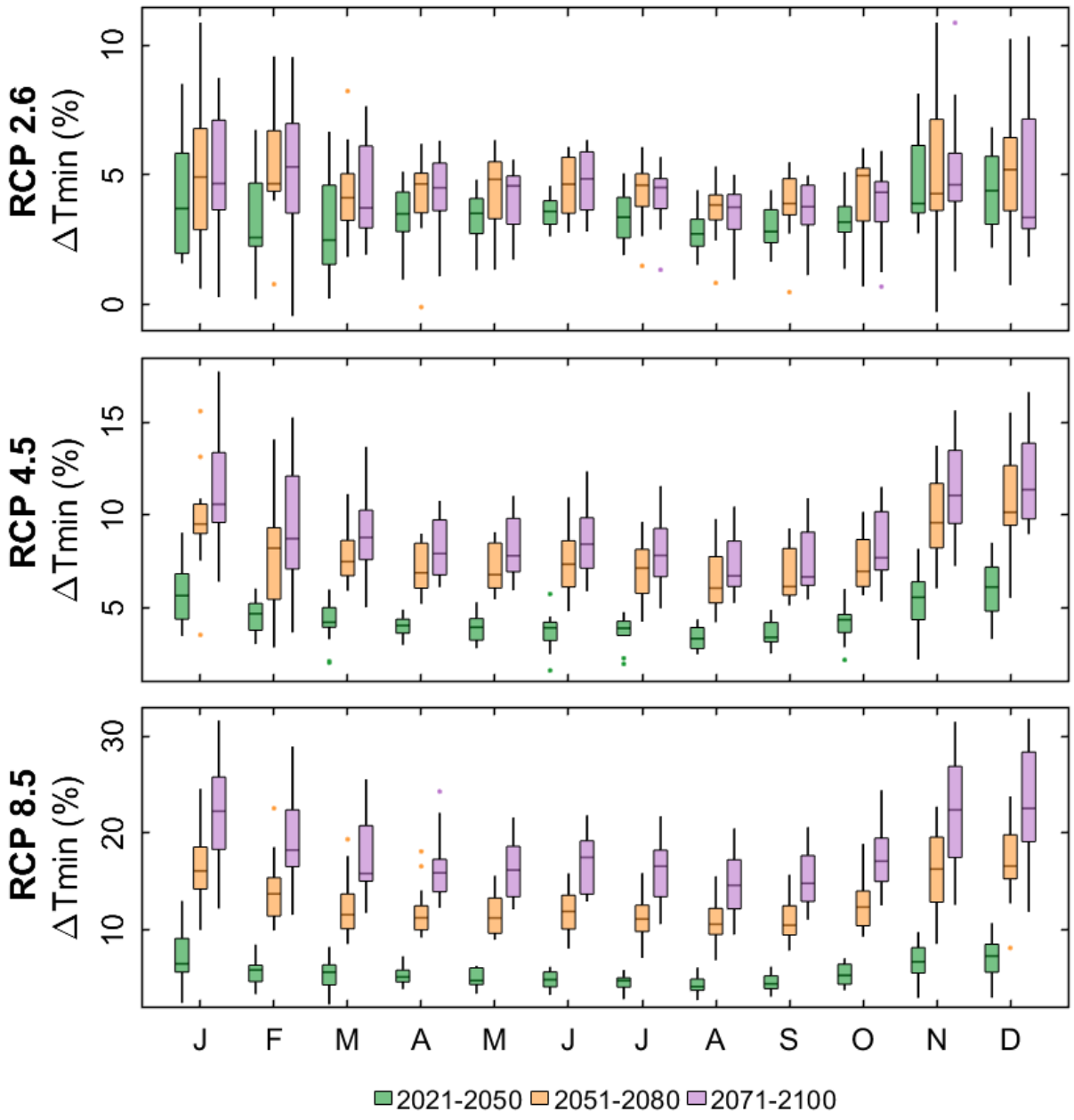

Figure S18. Percentage changes in annual cycles of minimum air temperature (ΔT_{min}) over the future periods in comparison to the historical period (1991-2020). Each boxplot represents the spread among the RCM-GCMs combinations under RCP2.6 (9 models), RCP4.5 (16 models) and RCP8.5 (18 models).

3.5 Potential evaporation

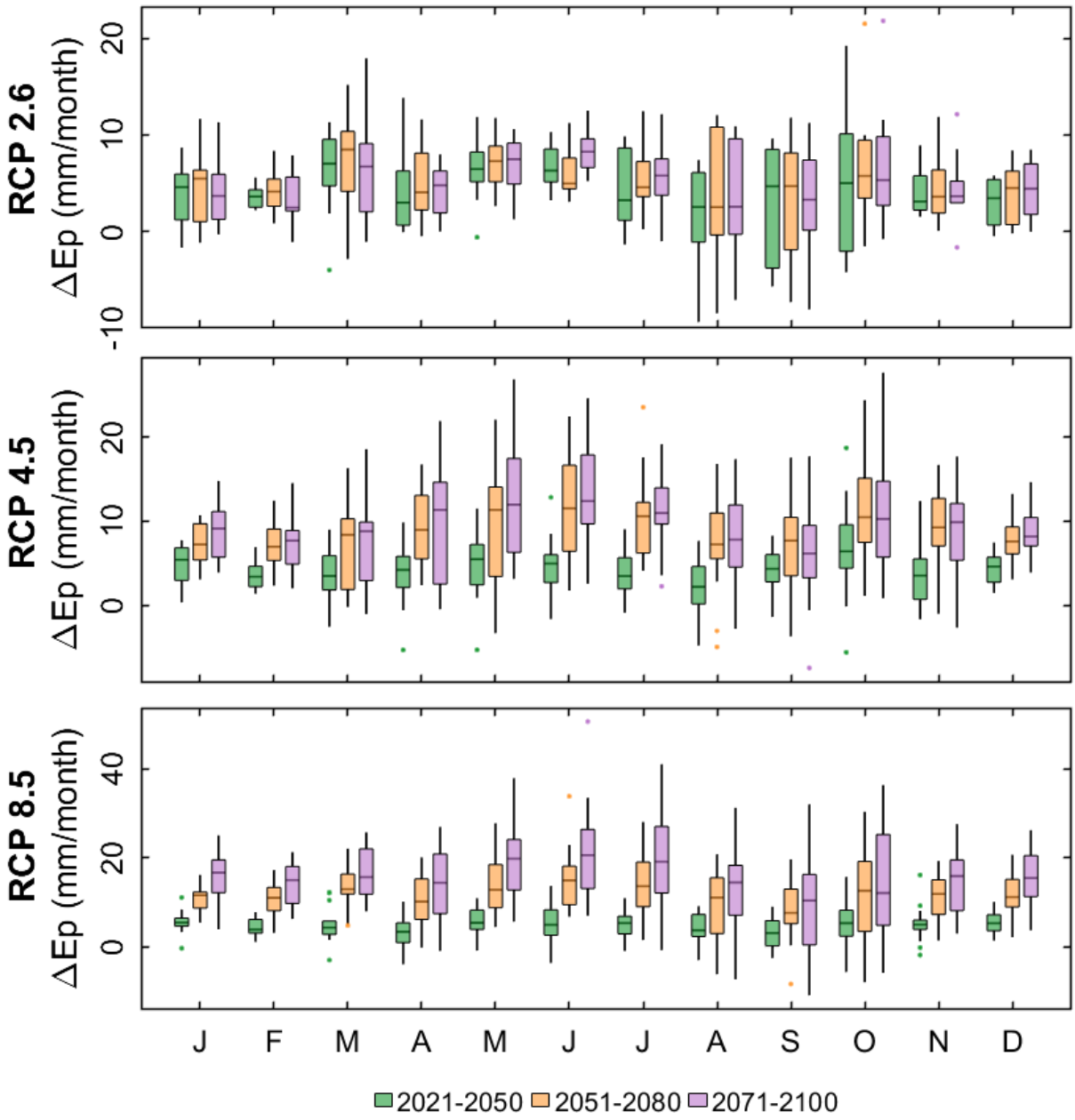

Figure S19. Changes in annual cycles of potential evaporation (ΔE_p) over the future periods in comparison to the historical period (1991-2020). Each boxplot represents the spread among the RCM-GCMs combinations under RCP2.6 (9 models), RCP4.5 (16 models) and RCP8.5 (18 models).

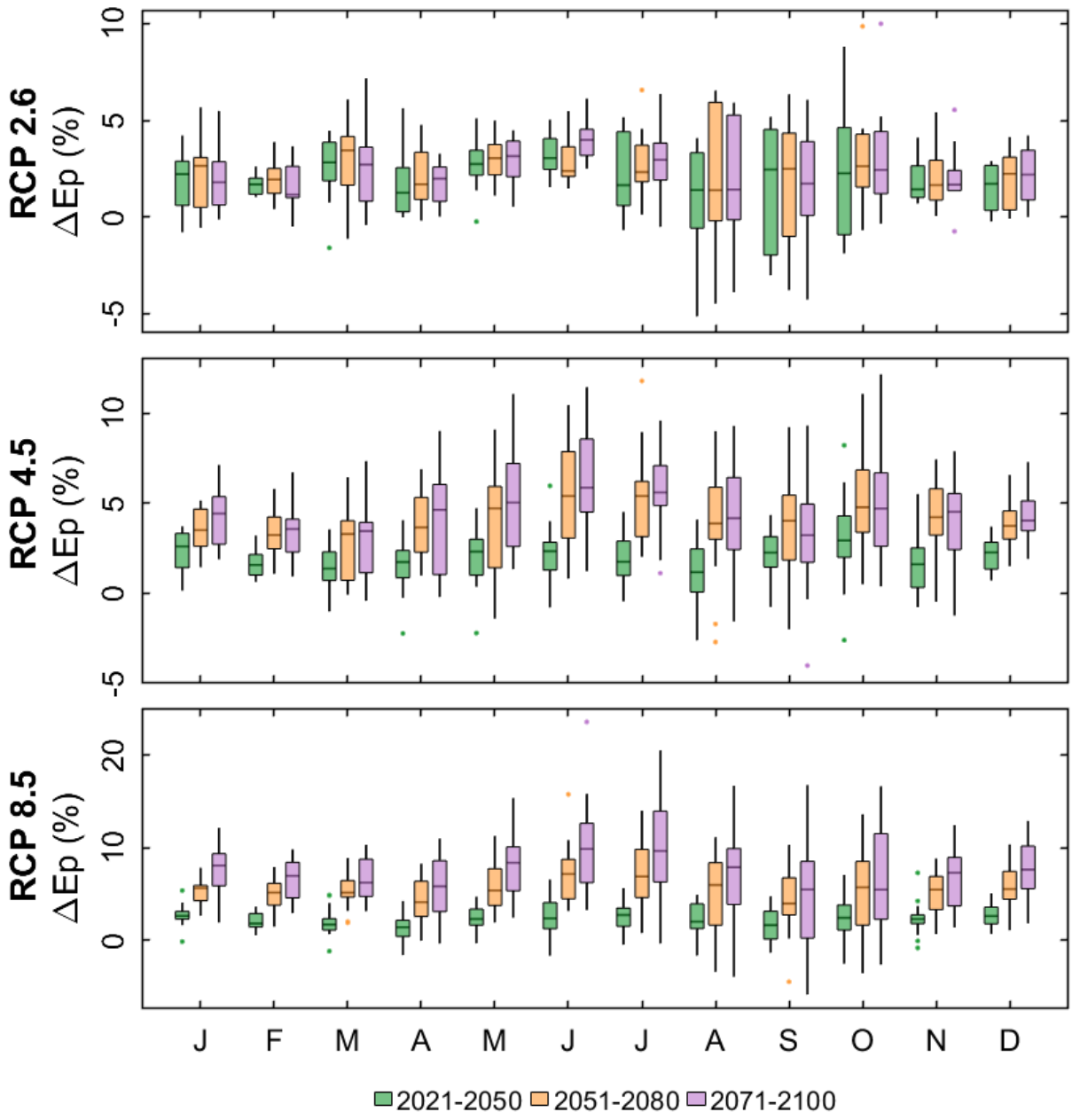

Figure S20. Percentage changes in annual cycles of potential evaporation (ΔE_p) over the future periods in comparison to the historical period (1991-2020). Each boxplot represents the spread among the RCM-GCMs combinations under RCP2.6 (9 models), RCP4.5 (16 models) and RCP8.5 (18 models).

3.6 Actual evaporation

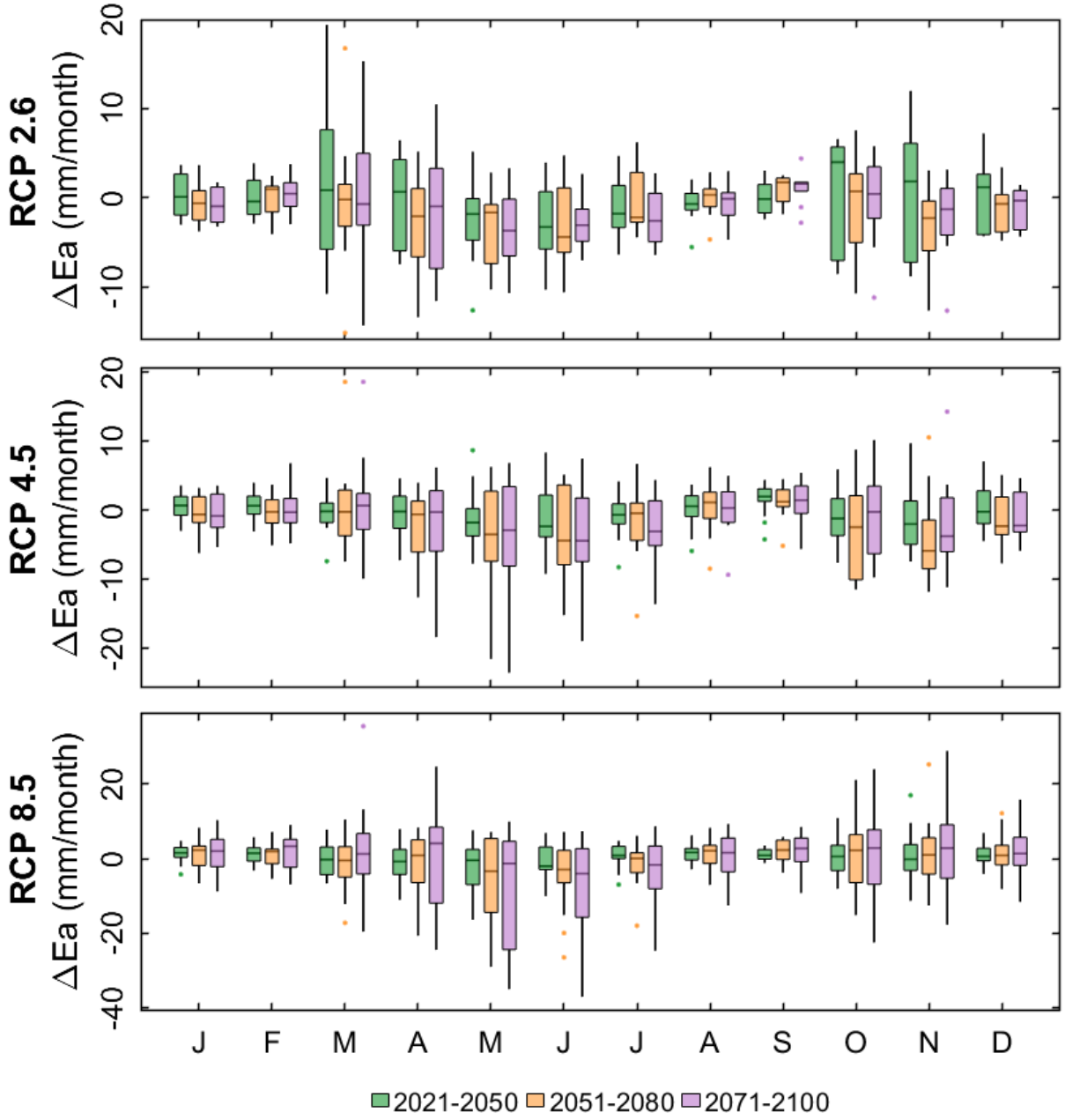

Figure S21. Changes in annual cycles of actual evaporation (Δ*E*a) over the future periods in comparison to the historical period (1991-2020). Each boxplot represents the spread among the RCM-GCMs combinations under RCP2.6 (9 models), RCP4.5 (16 models) and RCP8.5 (18 models).

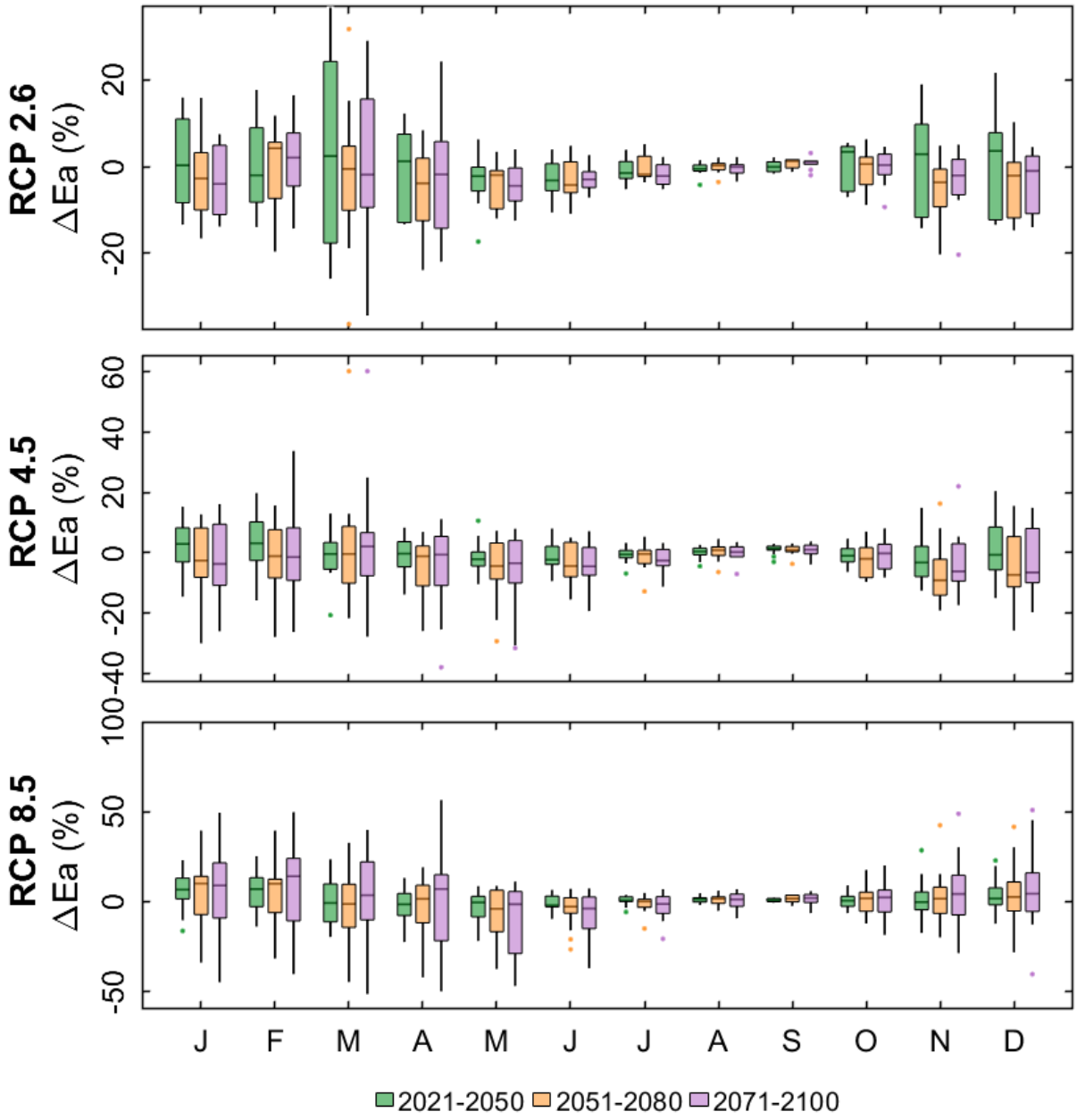

Figure S22. Percentage changes in annual cycles of actual evaporation (ΔE_a) over the future periods in comparison to the historical period (1991-2020). Each boxplot represents the spread among the RCM-GCMs combinations under RCP2.6 (9 models), RCP4.5 (16 models) and RCP8.5 (18 models).

3.7 Surface runoff

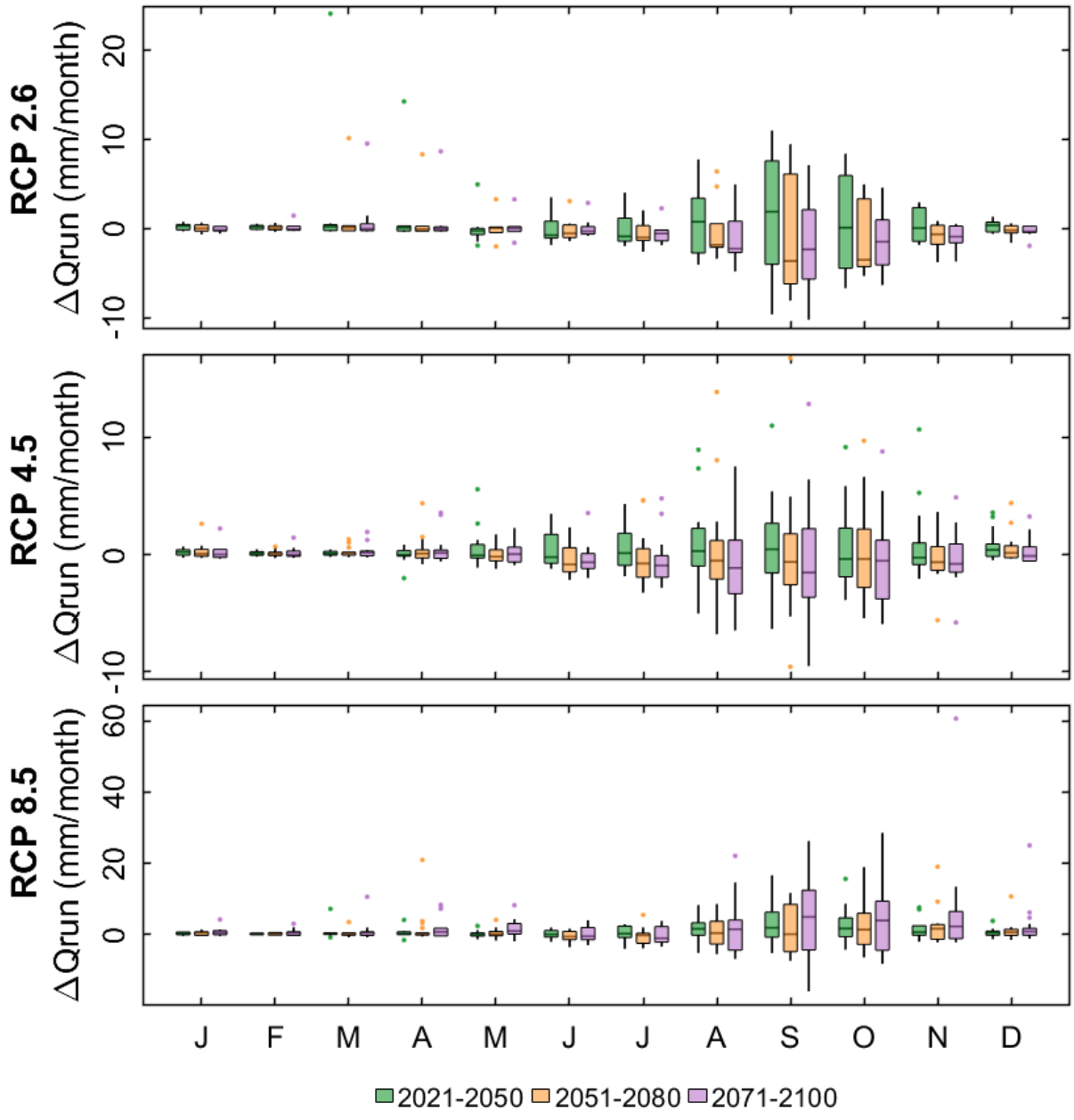

Figure S23. Changes in annual cycles of surface runoff (ΔQ_{run}) over the future periods in comparison to the historical period (1991-2020). Each boxplot represents the spread among the RCM-GCMs combinations under RCP2.6 (9 models), RCP4.5 (16 models) and RCP8.5 (18 models).

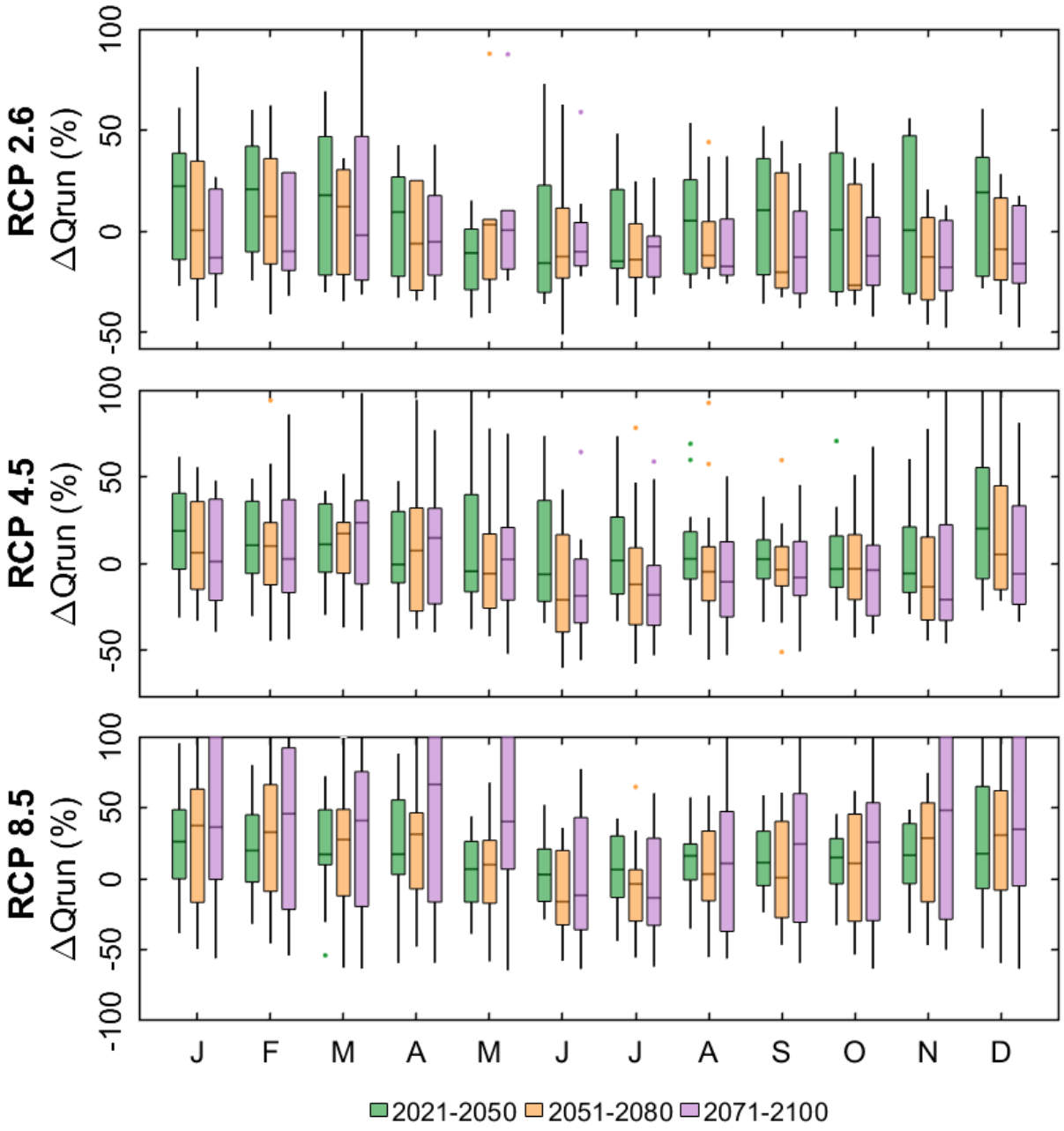

Figure S24. Percentage changes in annual cycles of surface runoff (ΔQ_{run}) over the future periods in comparison to the historical period (1991-2020). Each boxplot represents the spread among the RCM-GCMs combinations under RCP2.6 (9 models), RCP4.5 (16 models) and RCP8.5 (18 models).

3.8 Groundwater recharge

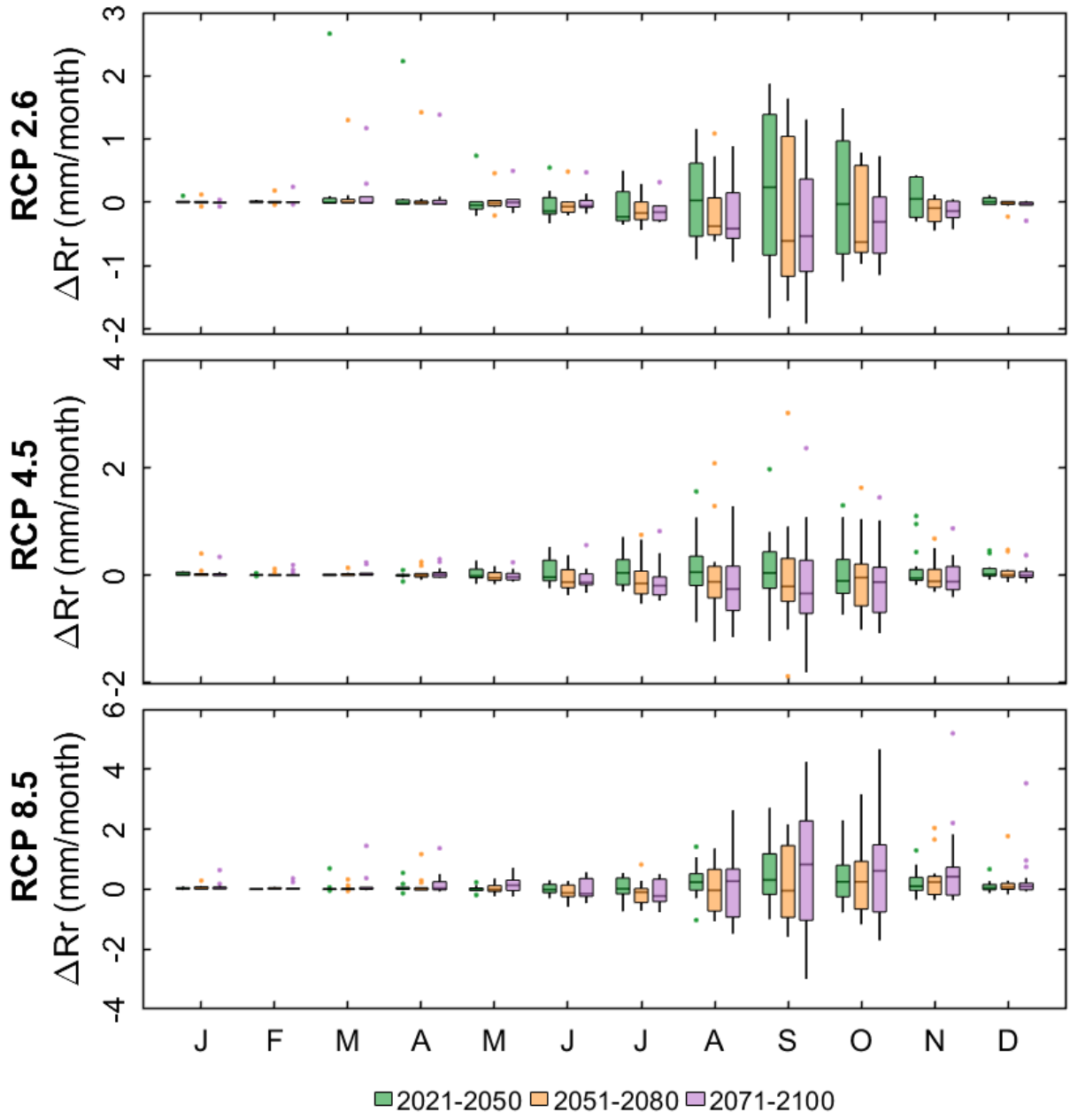

Figure S25. Changes in annual cycles of groundwater recharge (Δ*R*r) over the future periods in comparison to the historical period (1991-2020). Each boxplot represents the spread among the RCM-GCMs combinations under RCP2.6 (9 models), RCP4.5 (16 models) and RCP8.5 (18 models).

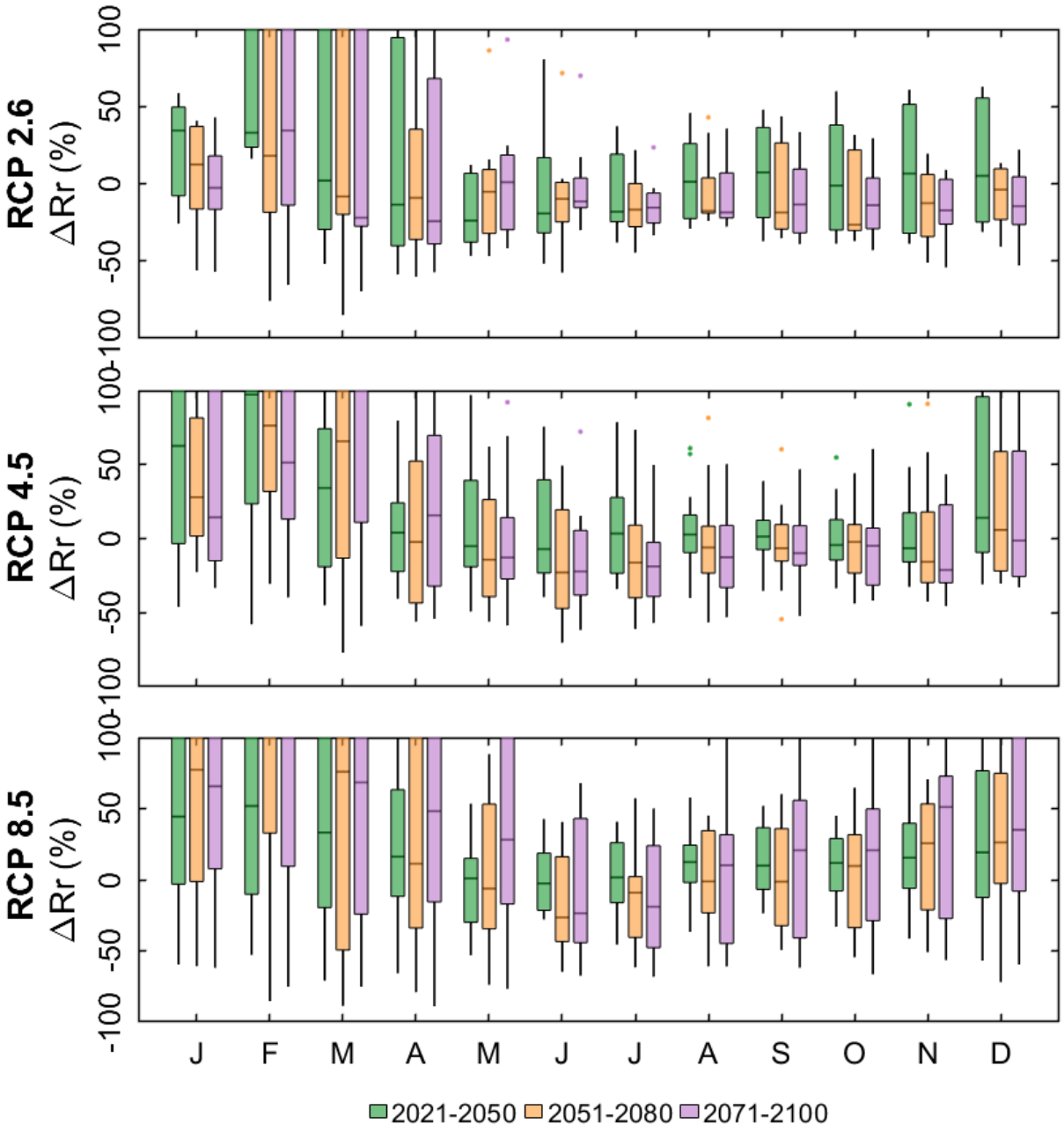

Figure S26. Percentage changes in annual cycles of groundwater recharge (Δ*R*r) over the future periods in comparison to the historical period (1991-2020). Each boxplot represents the spread among the RCM-GCMs combinations under RCP2.6 (9 models), RCP4.5 (16 models) and RCP8.5 (18 models).

3.9 Soil moisture

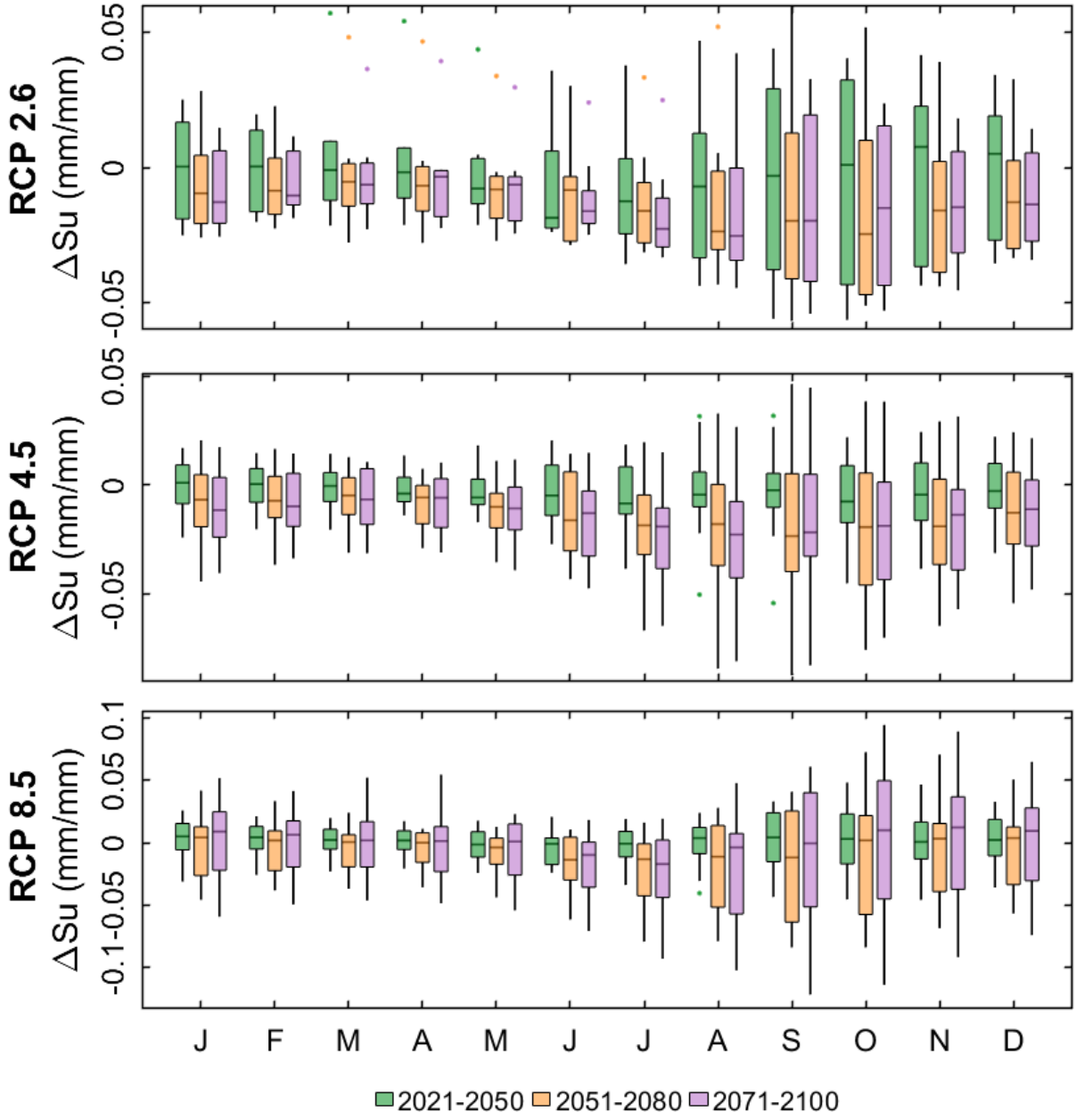

Figure S27. Changes in annual cycles of root-zone soil moisture (Δ*S*u) over the future periods in comparison to the historical period (1991-2020). Each boxplot represents the spread among the RCM-GCMs combinations under RCP2.6 (9 models), RCP4.5 (16 models) and RCP8.5 (18 models).

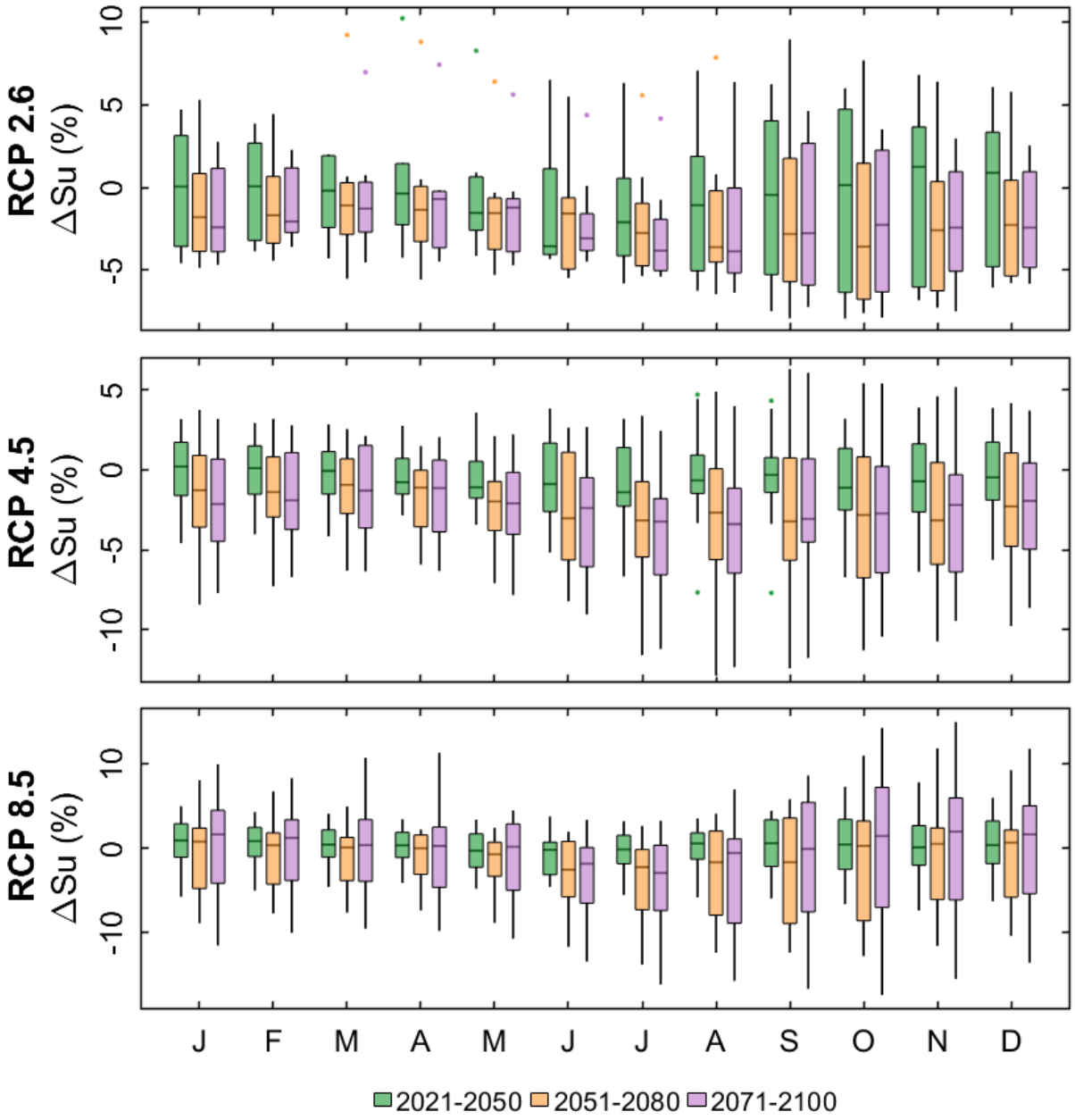

Figure S28. Percentage changes in annual cycles of root-zone soil moisture (Δ*Su*) over the future periods in comparison to the historical period (1991-2020). Each boxplot represents the spread among the RCM-GCMs combinations under RCP2.6 (9 models), RCP4.5 (16 models) and RCP8.5 (18 models).

3.10 Terrestrial water storage

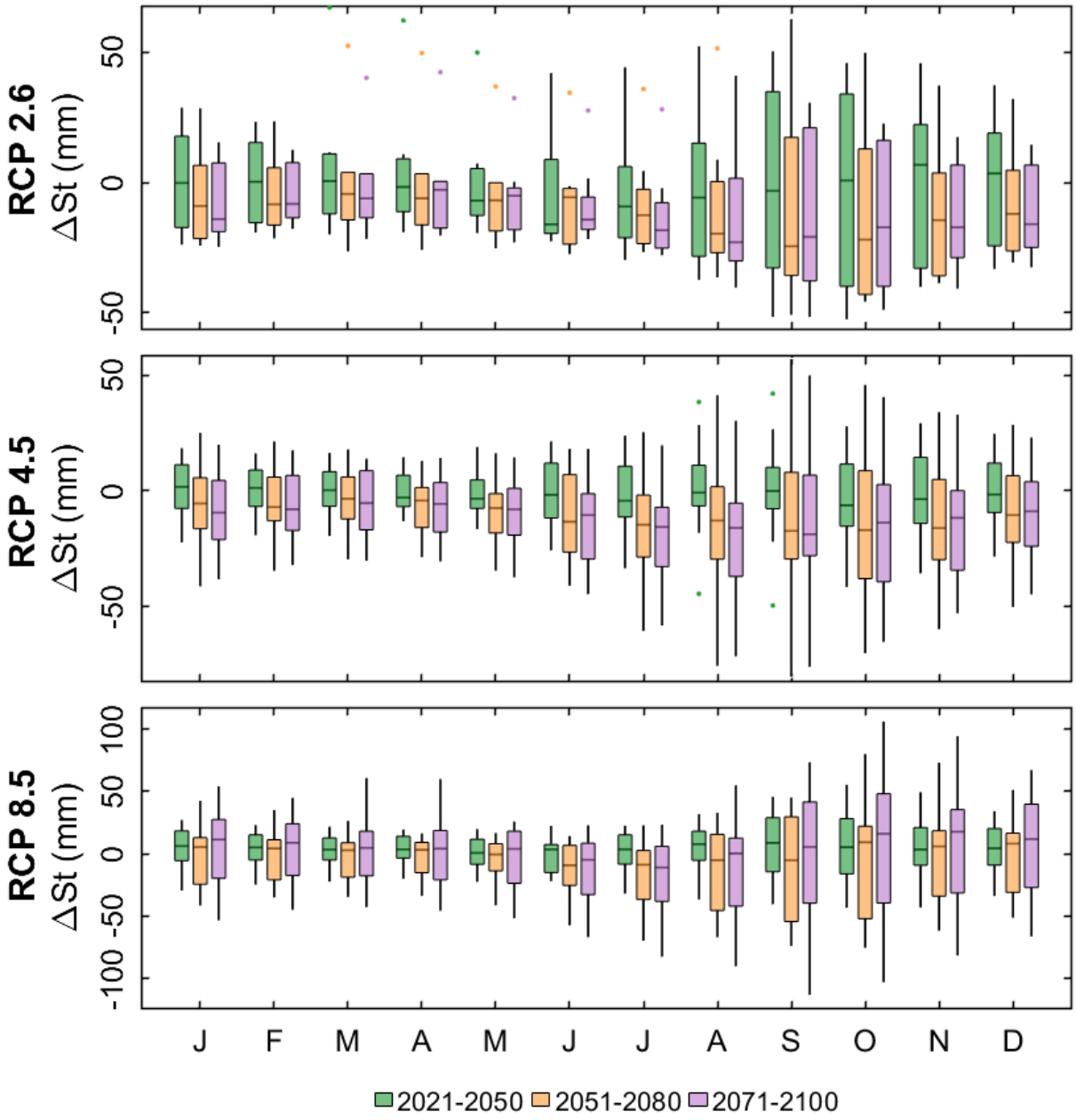

Figure S29. Changes in annual cycles of terrestrial water storage (Δ*S*t) over the future periods in comparison to the historical period (1991-2020). Each boxplot represents the spread among the RCM-GCMs combinations under RCP2.6 (9 models), RCP4.5 (16 models) and RCP8.5 (18 models).

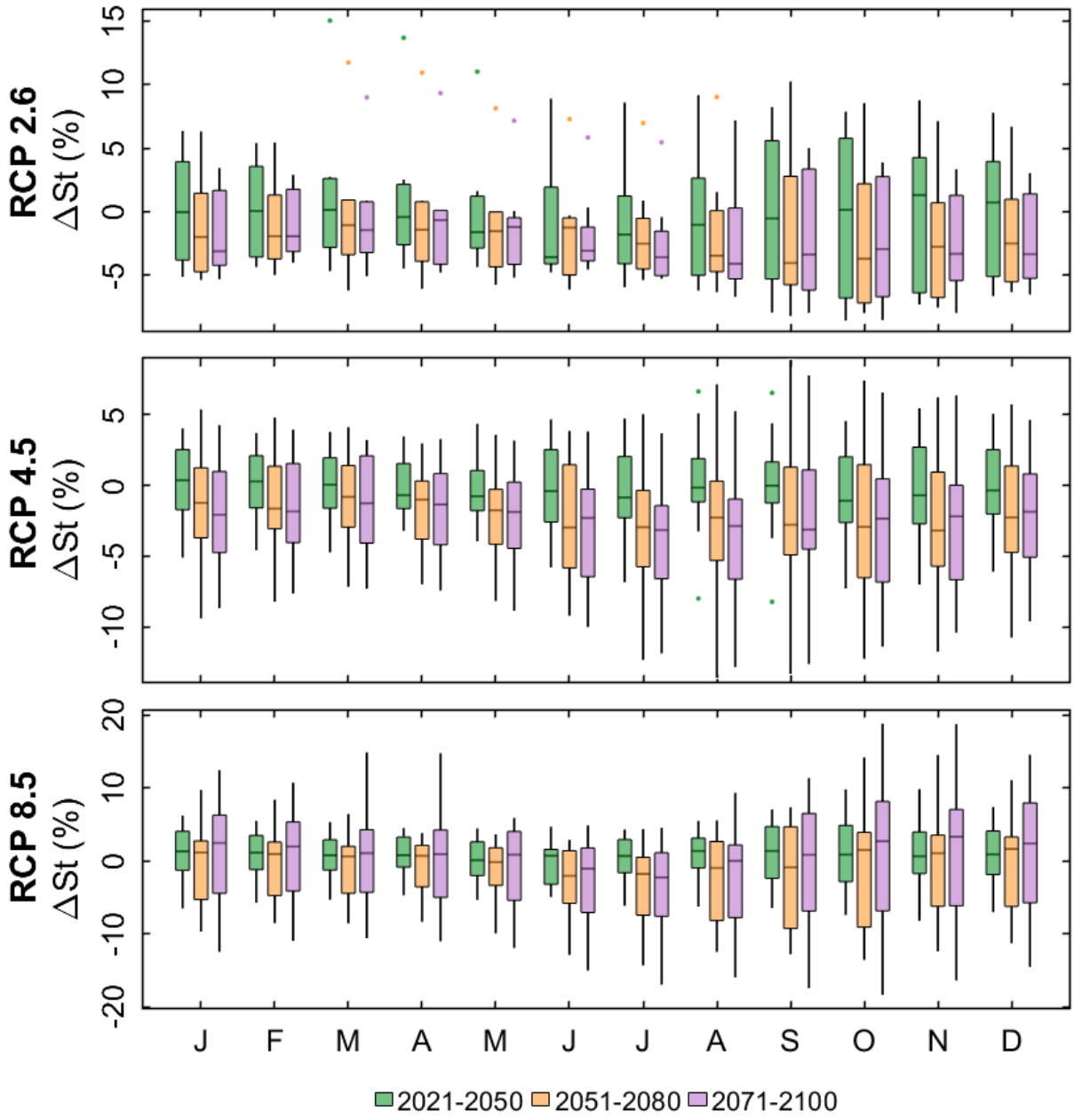

Figure S30. Percentage changes in annual cycles of terrestrial water storage (Δ*S*t) over the future periods in comparison to the historical period (1991-2020). Each boxplot represents the spread among the RCM-GCMs combinations under RCP2.6 (9 models), RCP4.5 (16 models) and RCP8.5 (18 models).

4 Inter-model variability

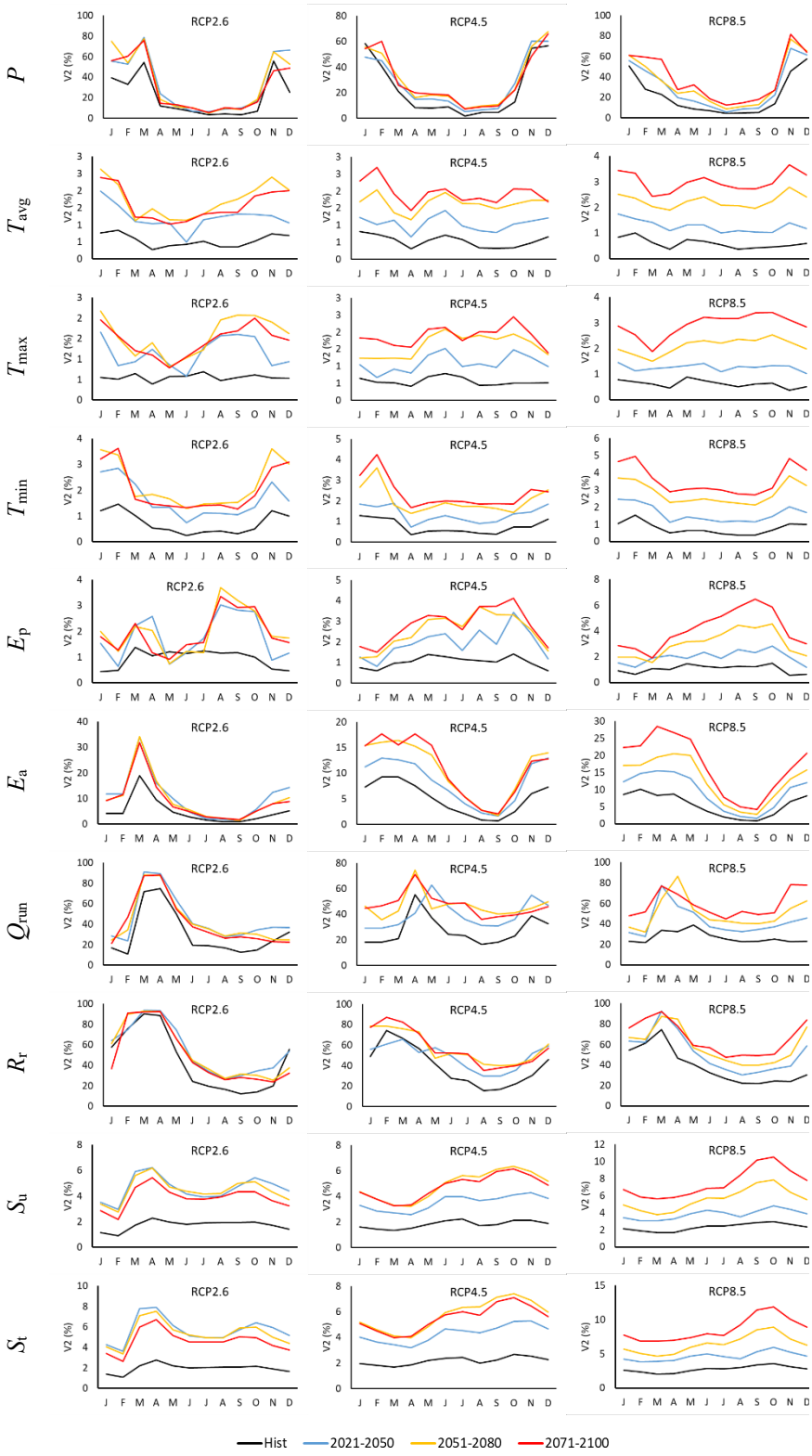

Figure S31. Inter-model (i.e., RCM-GCMs) variability expressed with the second-order coefficient of variation (V_2) for monthly hydroclimatic variables (T_{max}, T_{min}, T_{avg}, E_p, P, E_a, Q_{run}, R_r, S_u, and S_t) over the historical period (1991-2020) and the future period (2021-2100) under various RCPs.

5 Annual trends of hydroclimatic variables

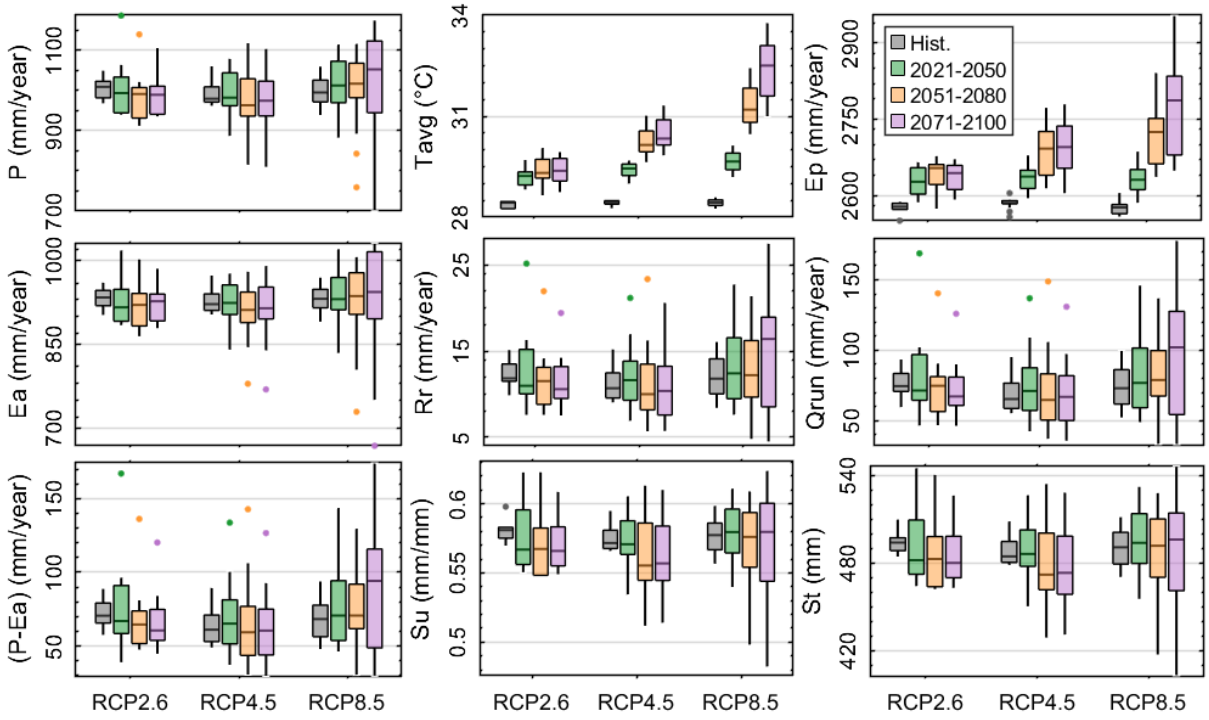

Figure S32. Annual trends in hydroclimatic variables over the historical (1991-2020) and future periods. Each boxplot represents the spread among the RCM-GCMs combinations under RCP2.6 (9 models), RCP4.5 (16 models) and RCP8.5 (18 models).

6 Spatial patterns of hydroclimatic variables across climatic zones

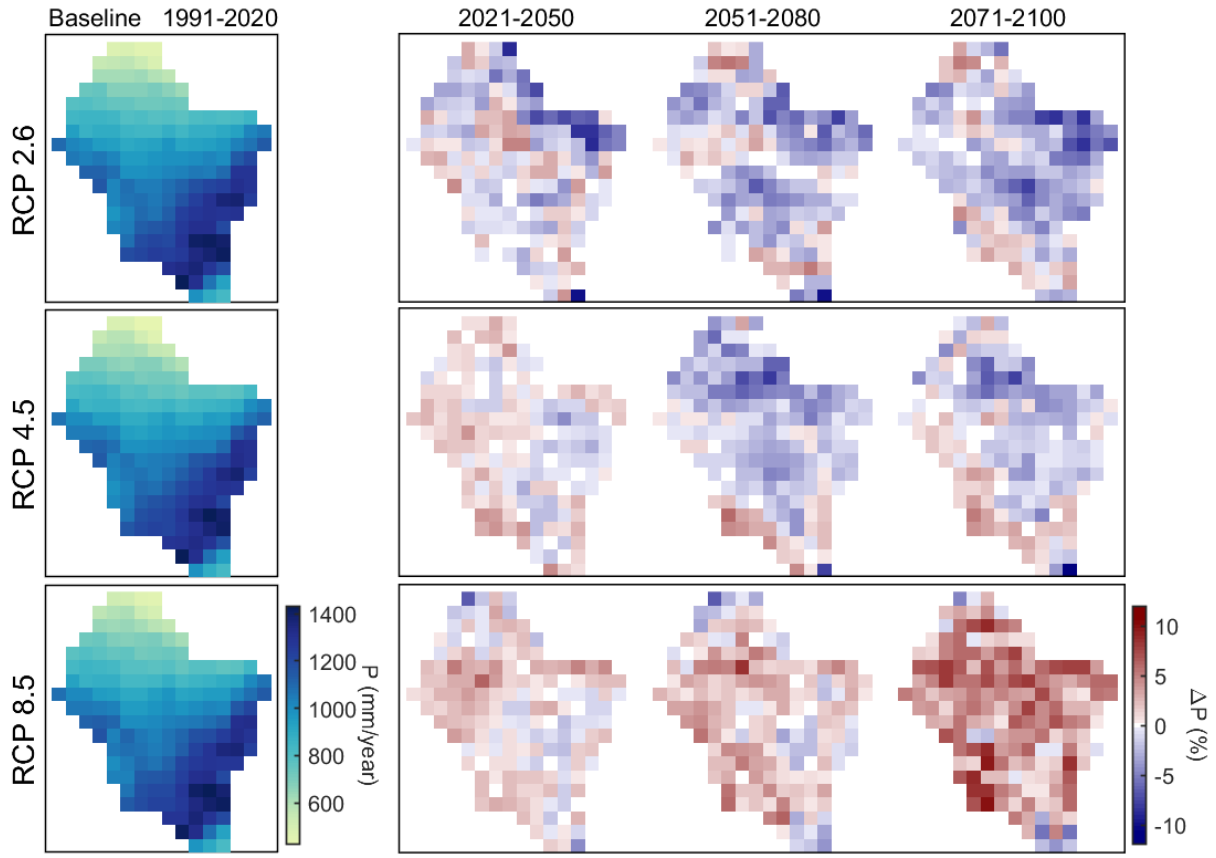

Figure S33. Spatial patterns of the long-term average of annual rainfall (*P*) over the historical period (1991-2020) and changes over future periods (2021-2100).

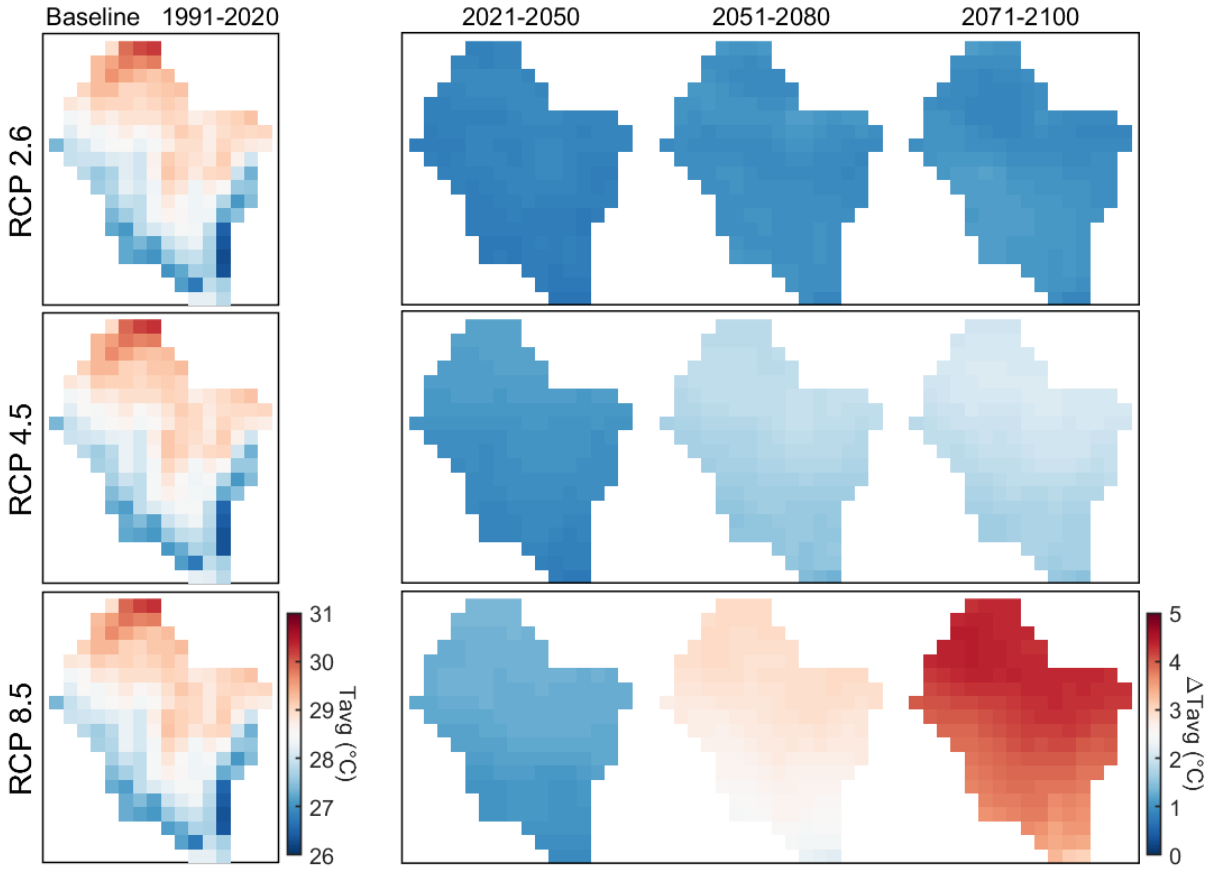

Figure S34. Spatial patterns of the long-term average of annual average air temperature (T_{avg}) over the historical period (1991-2020) and changes over future periods (2021-2100).

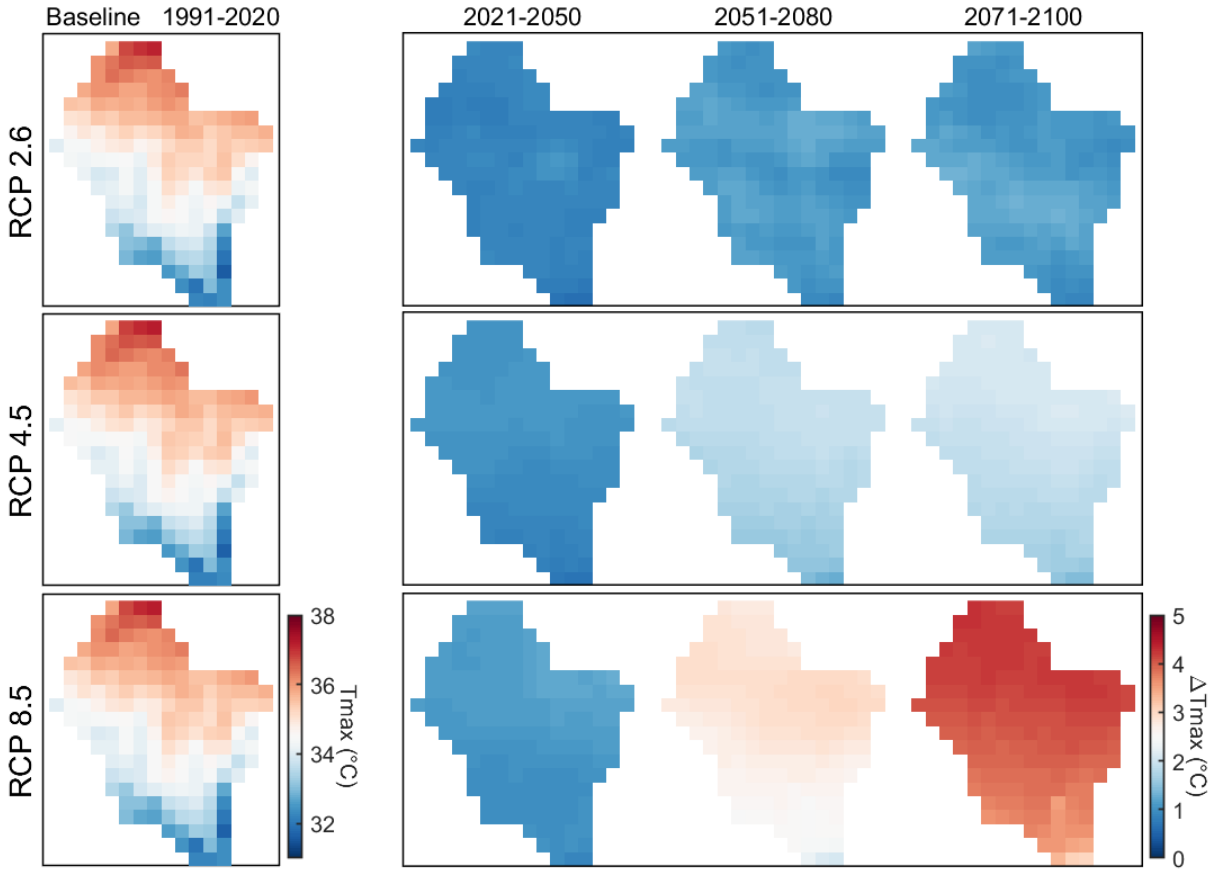

Figure S35. Spatial patterns of the long-term average of annual maximum air temperature (T_{max}) over the historical period (1991-2020) and changes over future periods (2021-2100).

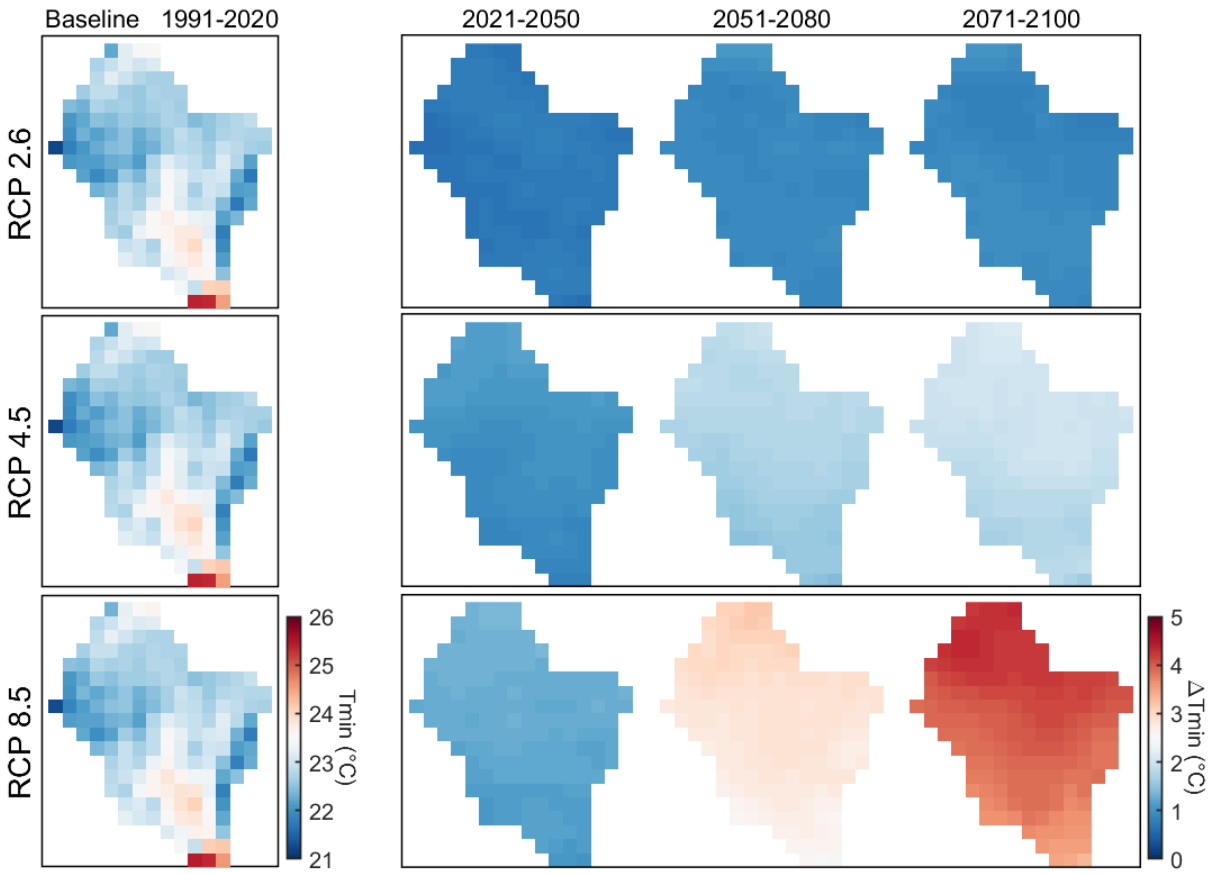

Figure S36. Spatial patterns of the long-term average of annual minimum air temperature (T_{min}) over the historical period (1991-2020) and changes over future periods (2021-2100).

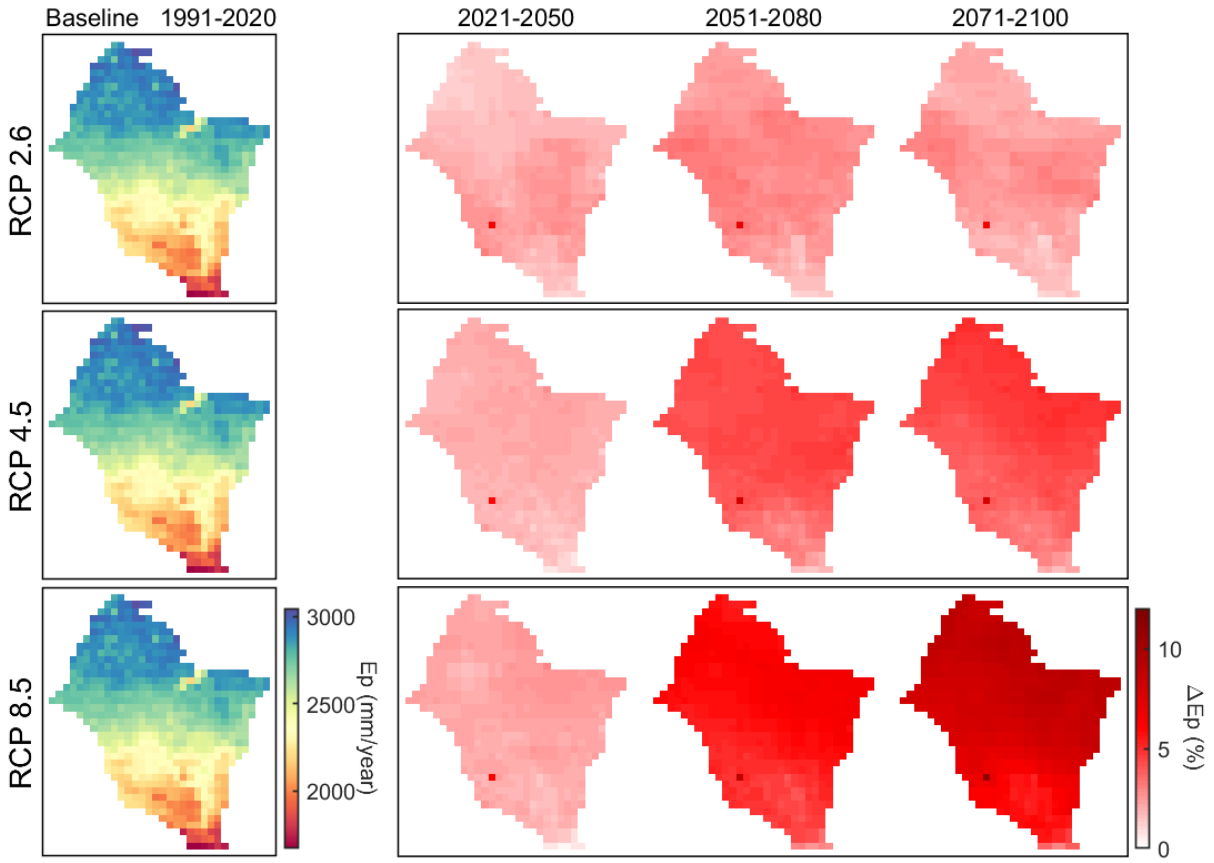

Figure S37. Spatial patterns of the long-term average of annual potential evaporation (E_p) over the historical period (1991-2020) and changes over future periods (2021-2100).

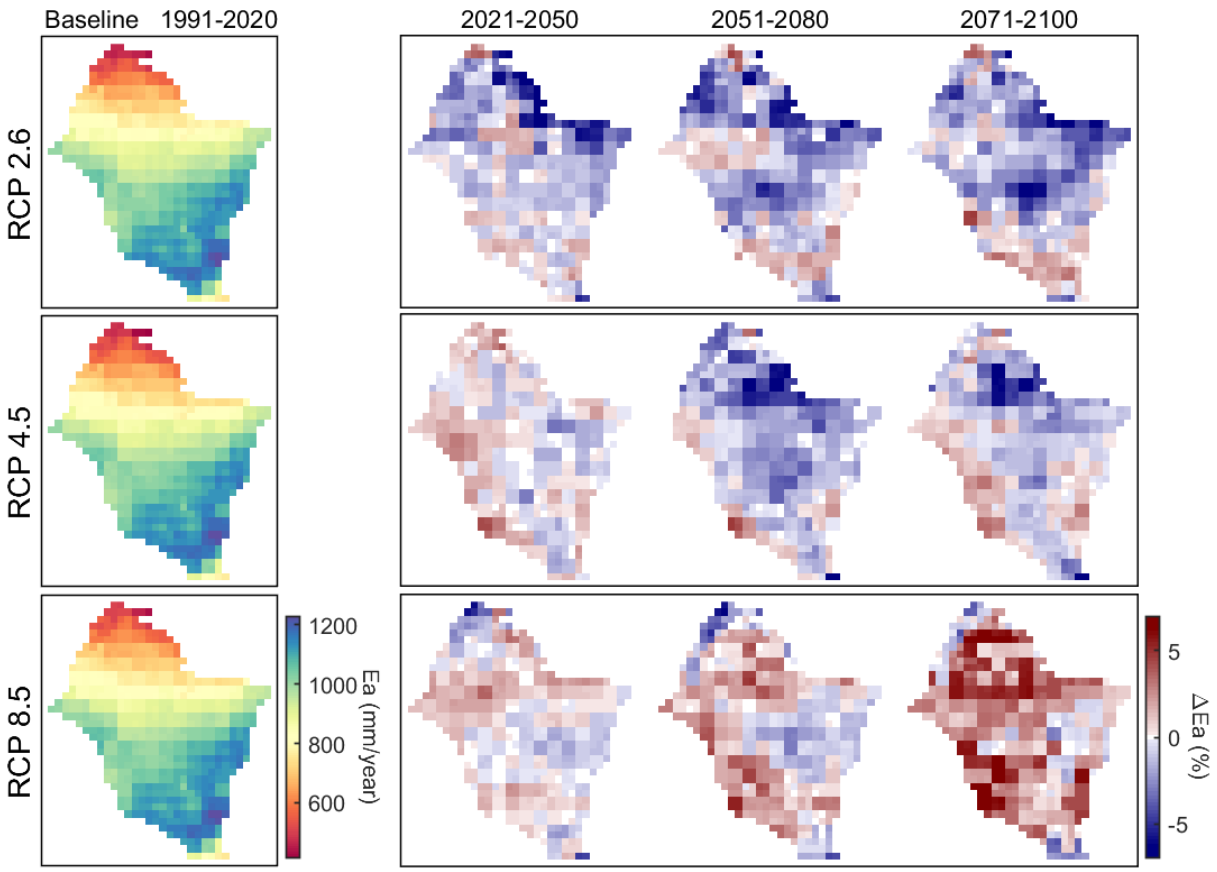

Figure S38. Spatial patterns of the long-term average of annual actual evaporation (E_a) over the historical period (1991-2020) and changes over future periods (2021-2100).

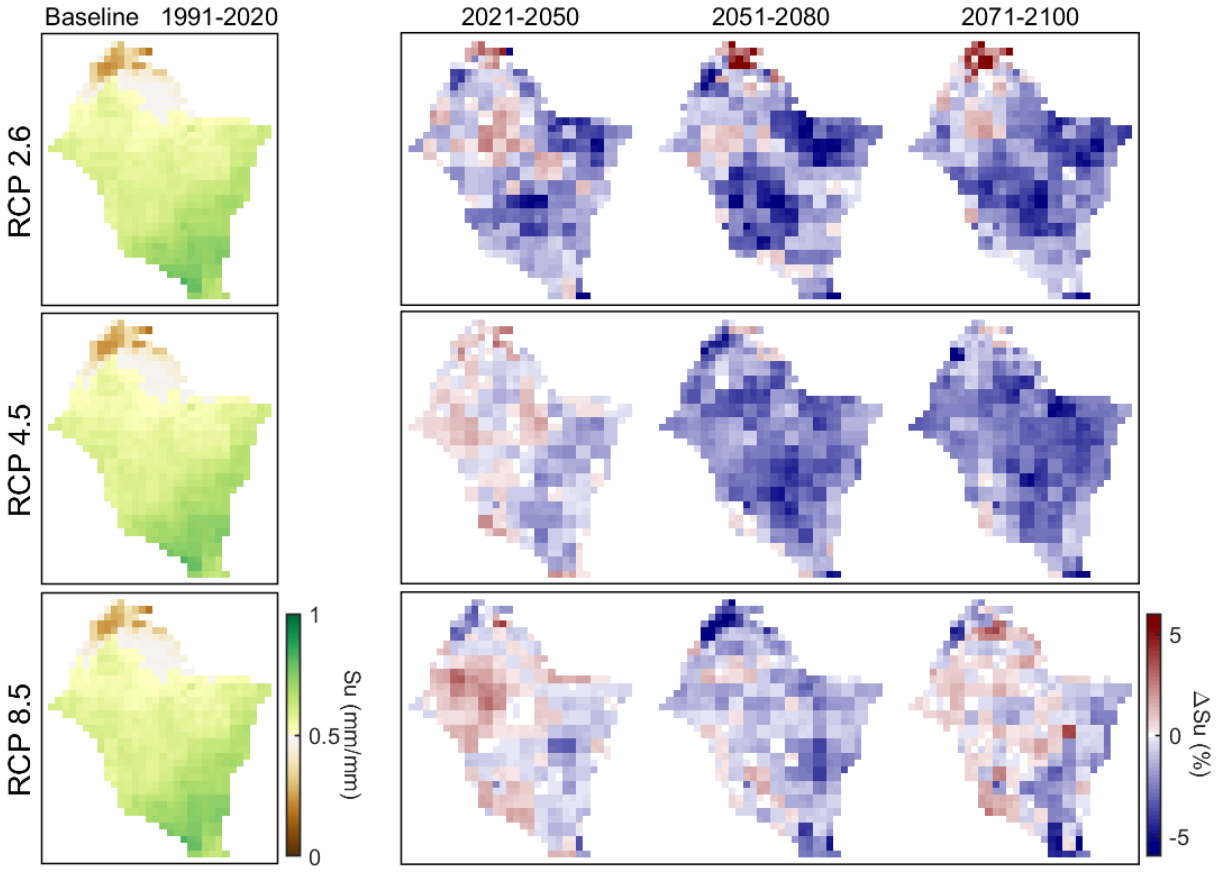

Figure S39. Spatial patterns of the long-term average of annual root-zone soil moisture (S_u) over the historical period (1991-2020) and changes over future periods (2021-2100).

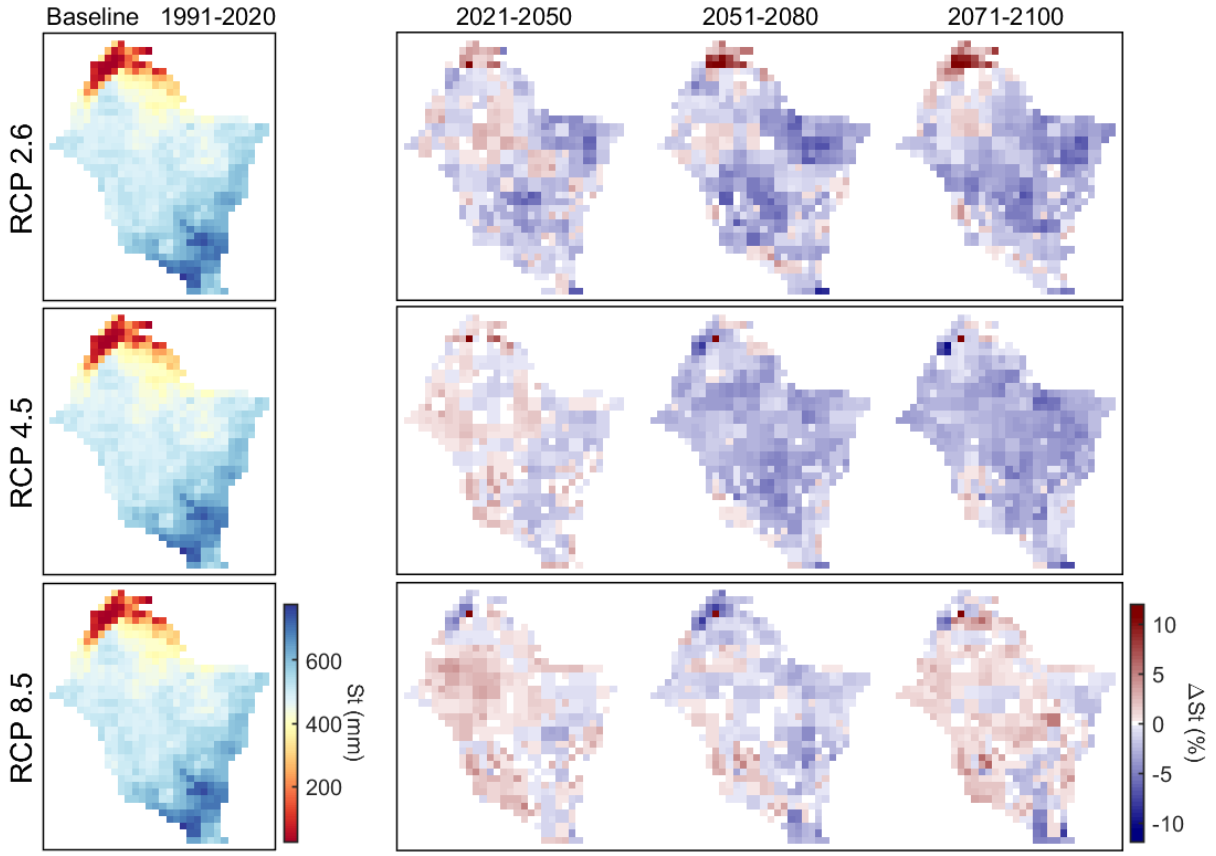

Figure S40. Spatial patterns of the long-term average of annual terrestrial water storage (S_t) over the historical period (1991-2020) and changes over future periods (2021-2100).

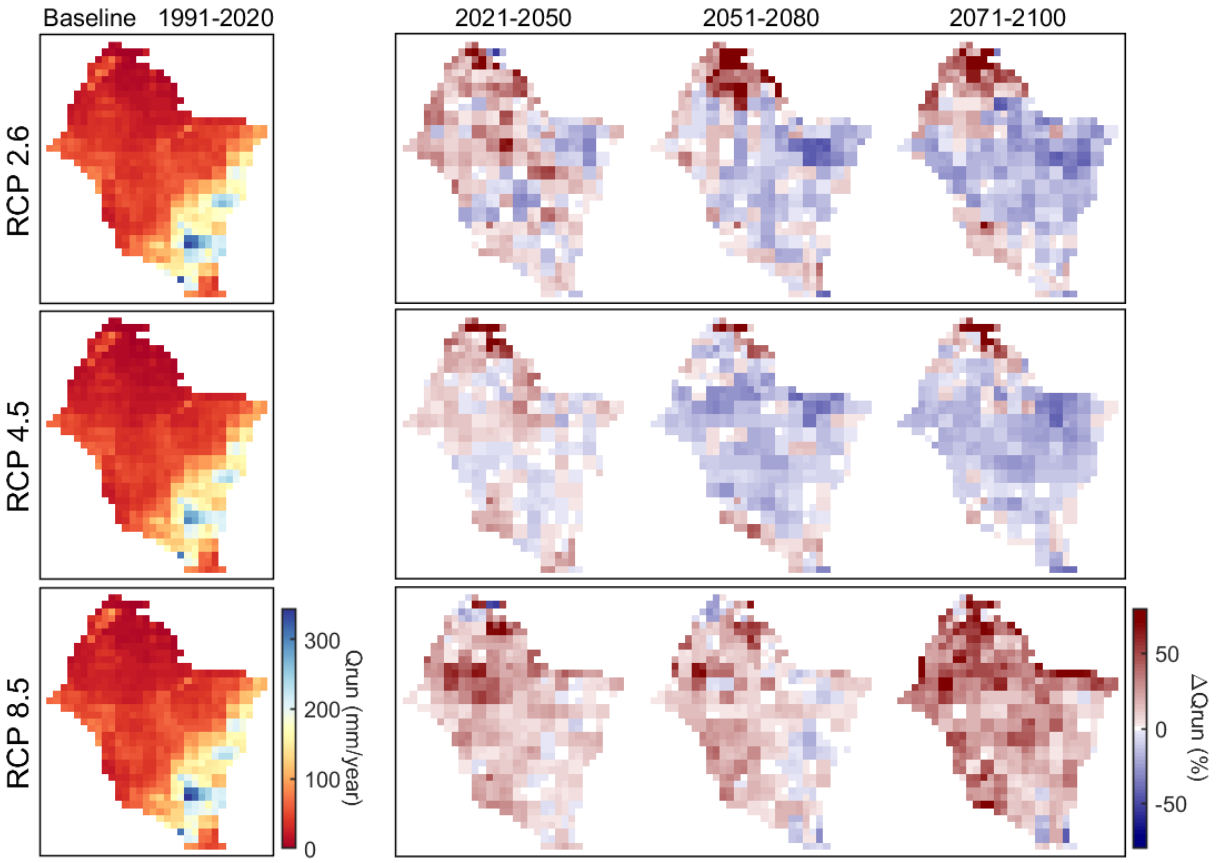

Figure S41. Spatial patterns of the long-term average of annual total runoff (Q_{run}) over the historical period (1991-2020) and changes over future periods (2021-2100).

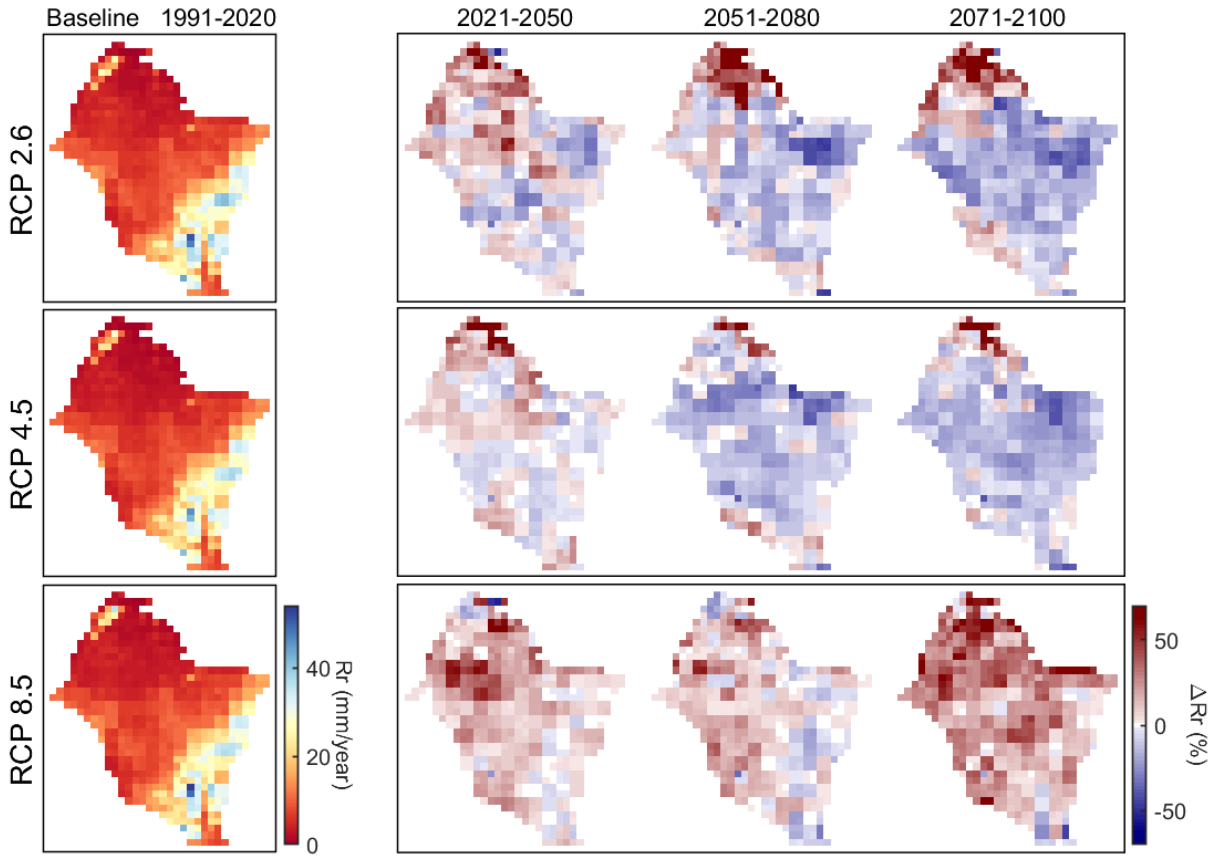

Figure S42. Spatial patterns of the long-term average of annual groundwater recharge (R_r) over the historical period (1991-2020) and changes over future periods (2021-2100).

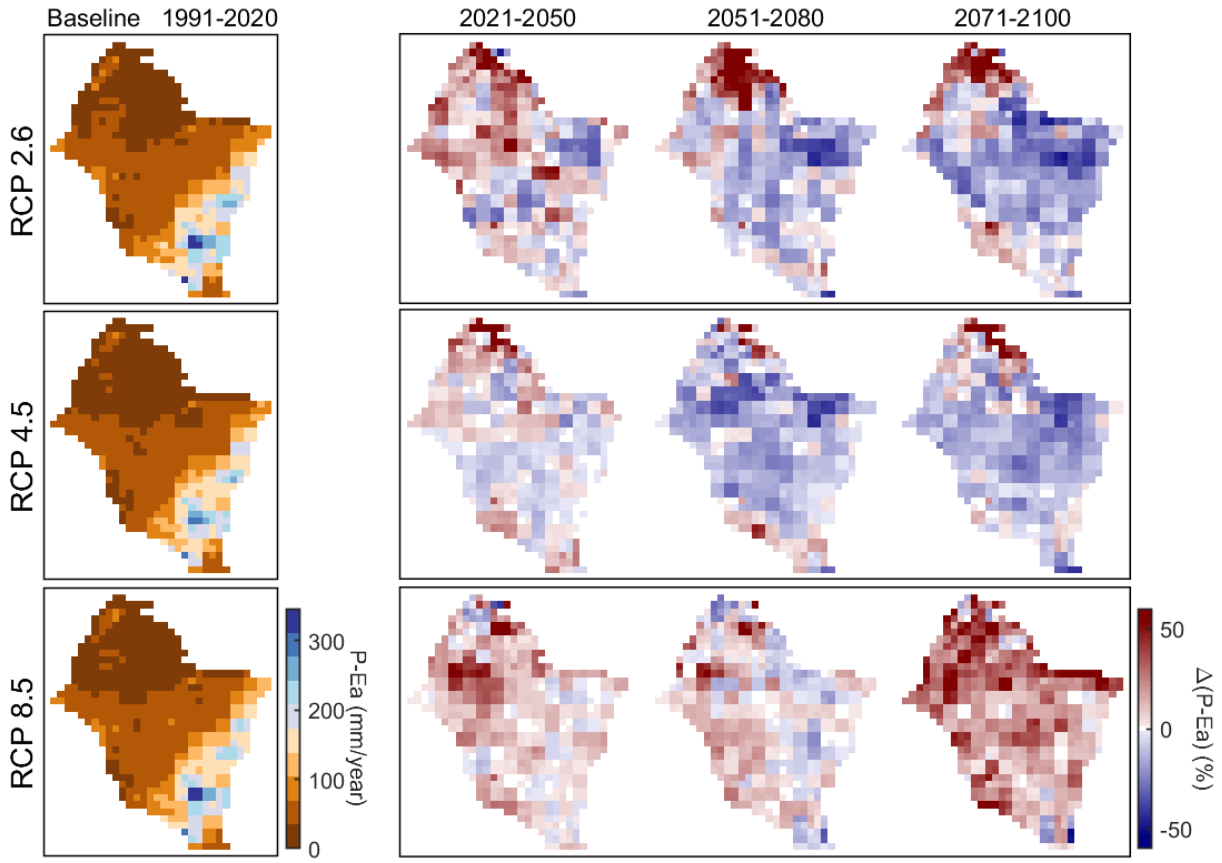

Figure S43. Spatial patterns of the long-term average of annual water availability (P-E_a) over the historical period (1991-2020) and changes over future periods (2021-2100).

7 Spatial patterns of inter-model variability across climatic zones

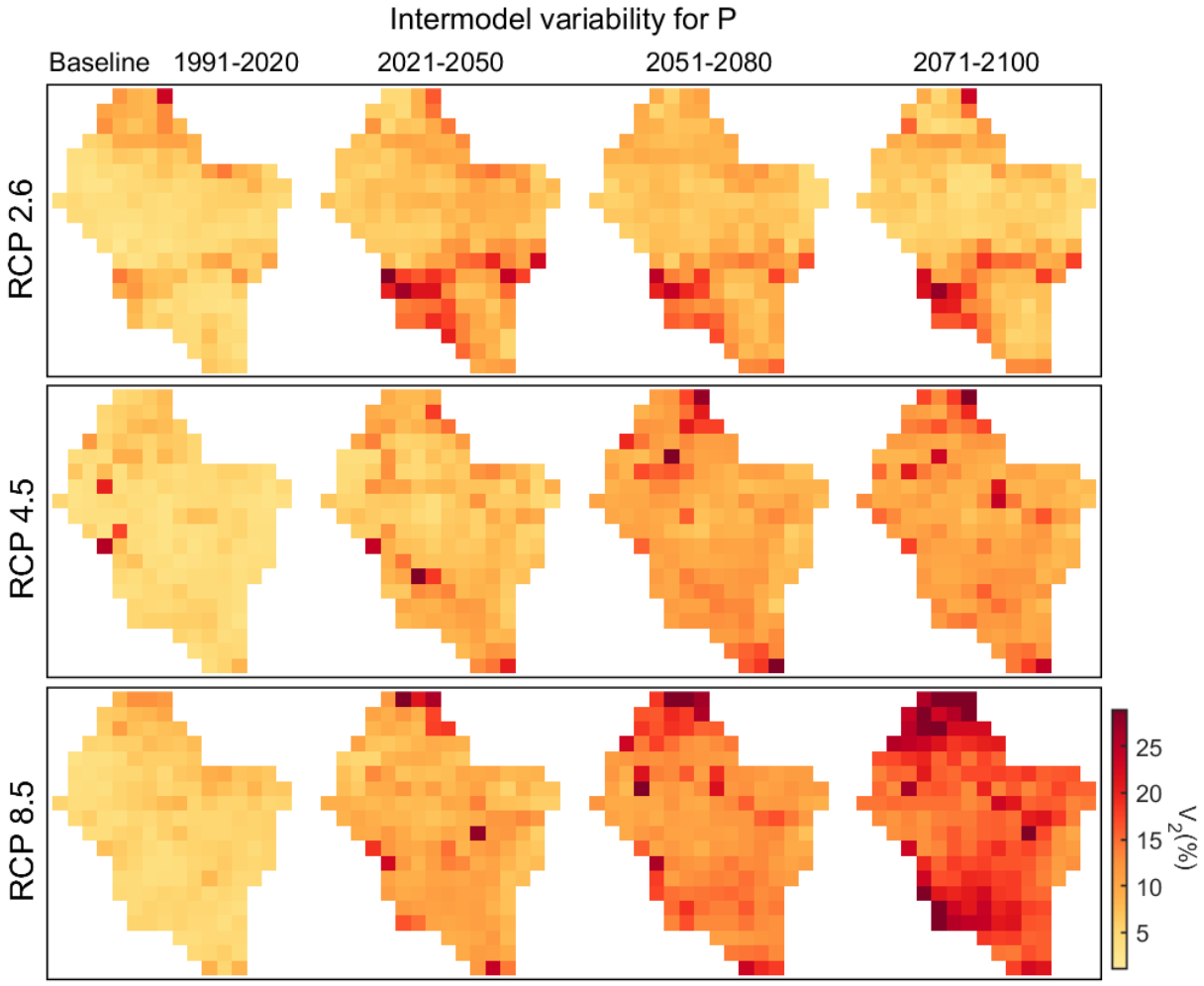

Figure S44. Spatial patterns of inter-model variability of annual rainfall (*P*).

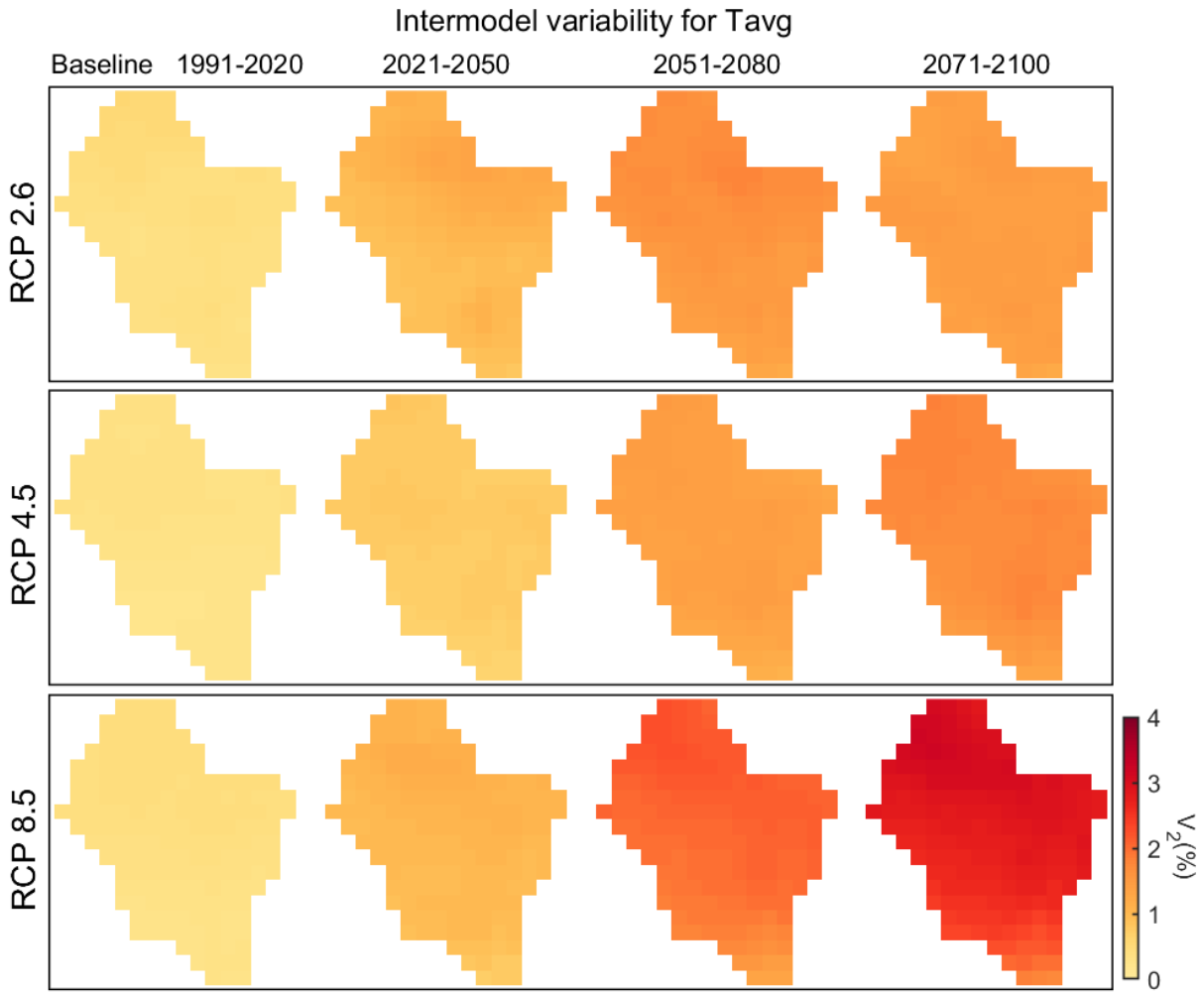

Figure S45. Spatial patterns of inter-model variability of annual average air temperature (T_{avg}).

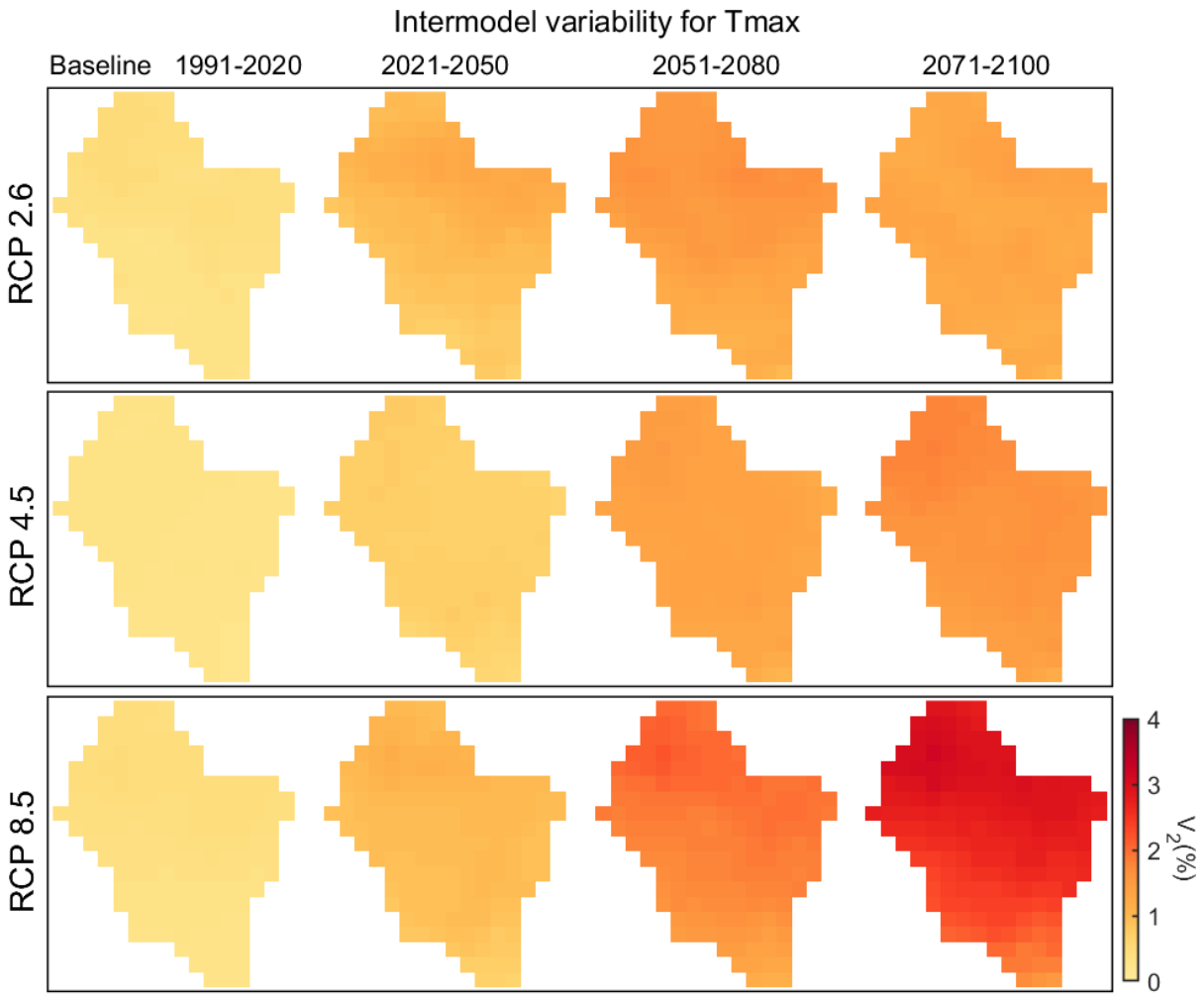

Figure S46. Spatial patterns of inter-model variability of annual maximum air temperature (T_{max}).

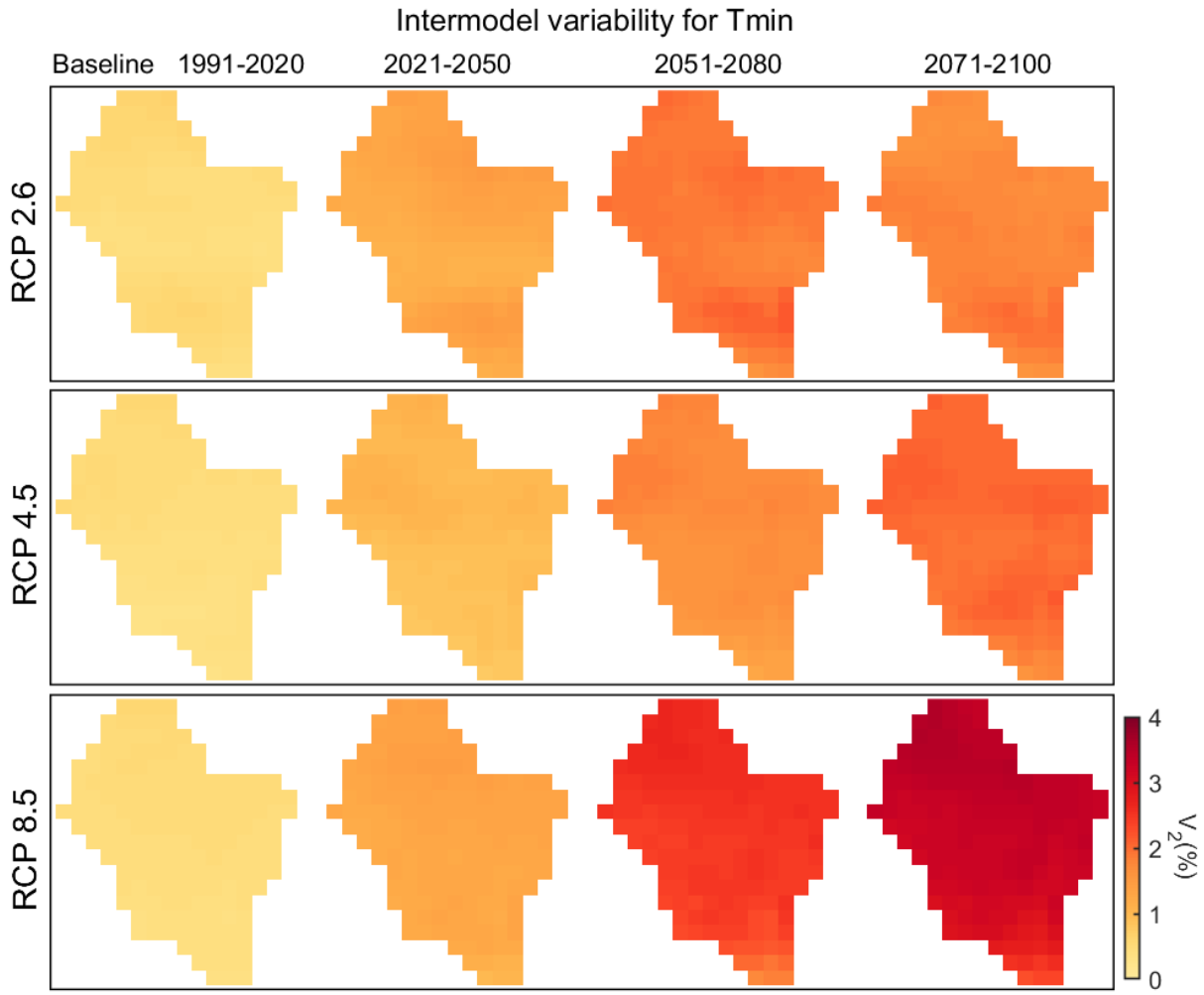

Figure S47. Spatial patterns of inter-model variability of annual minimum air temperature (T_{min}).

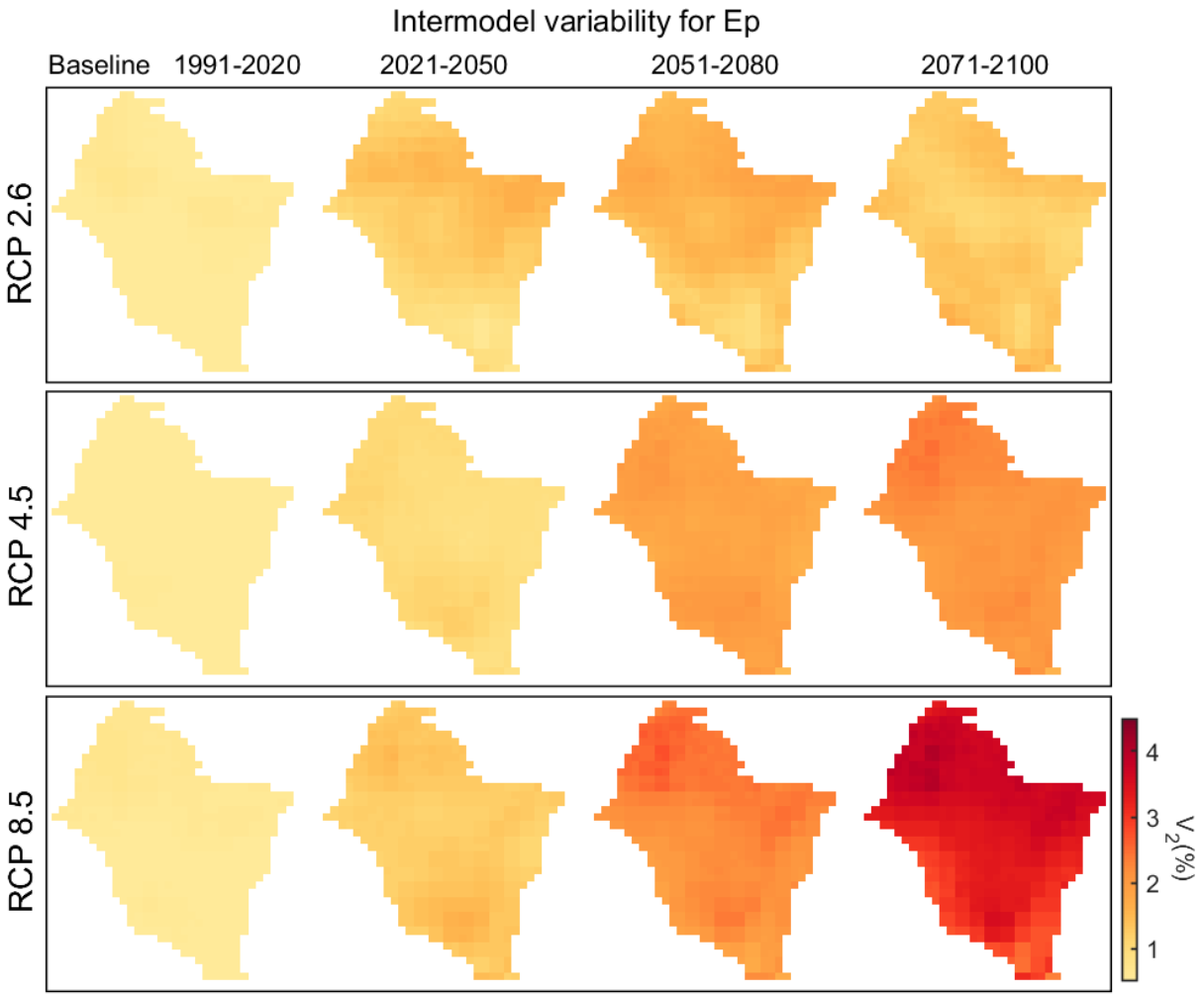

Figure S48. Spatial patterns of inter-model variability of annual potential evaporation (E_p).

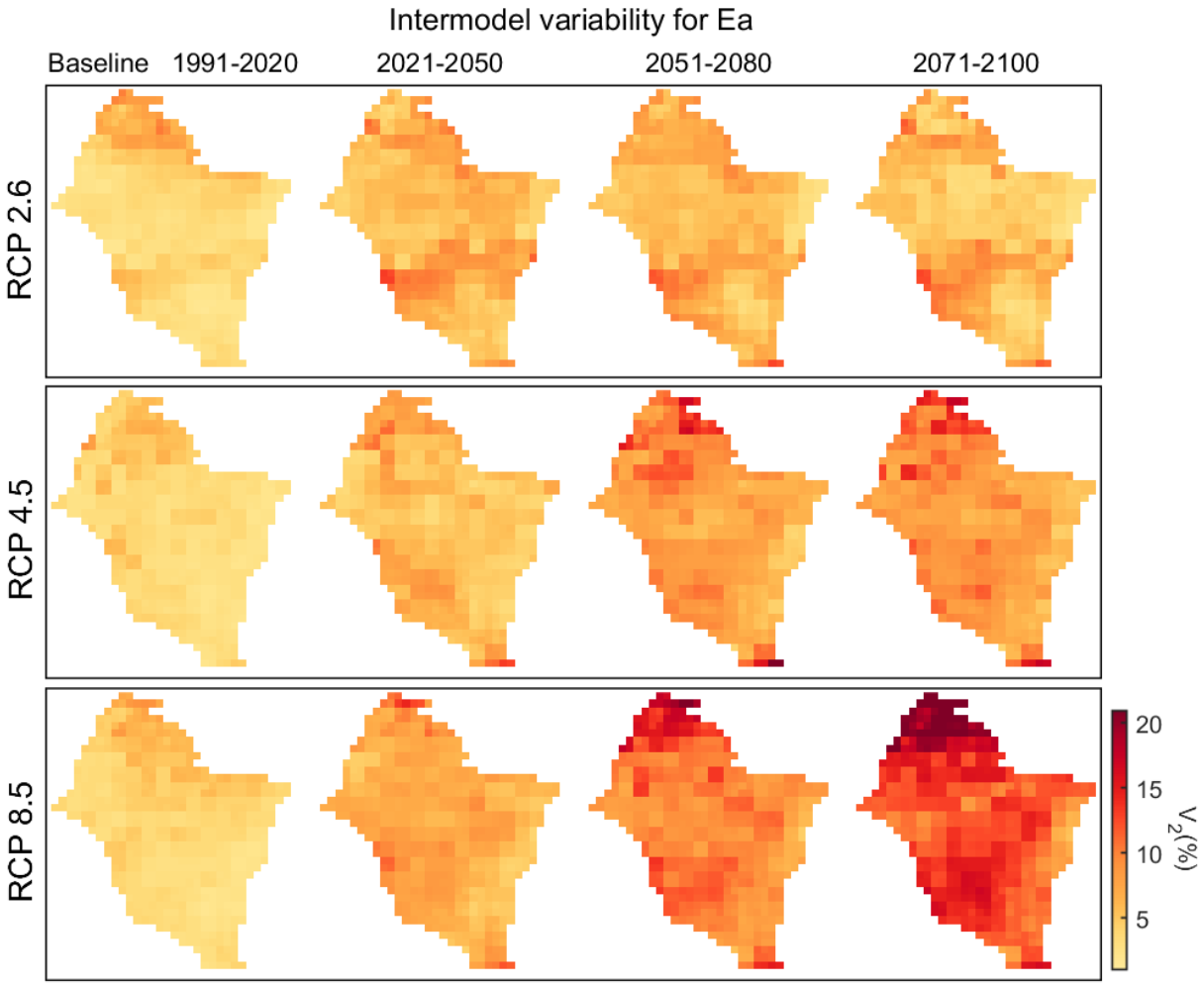

Figure S49. Spatial patterns of inter-model variability of annual actual evaporation (E_a).

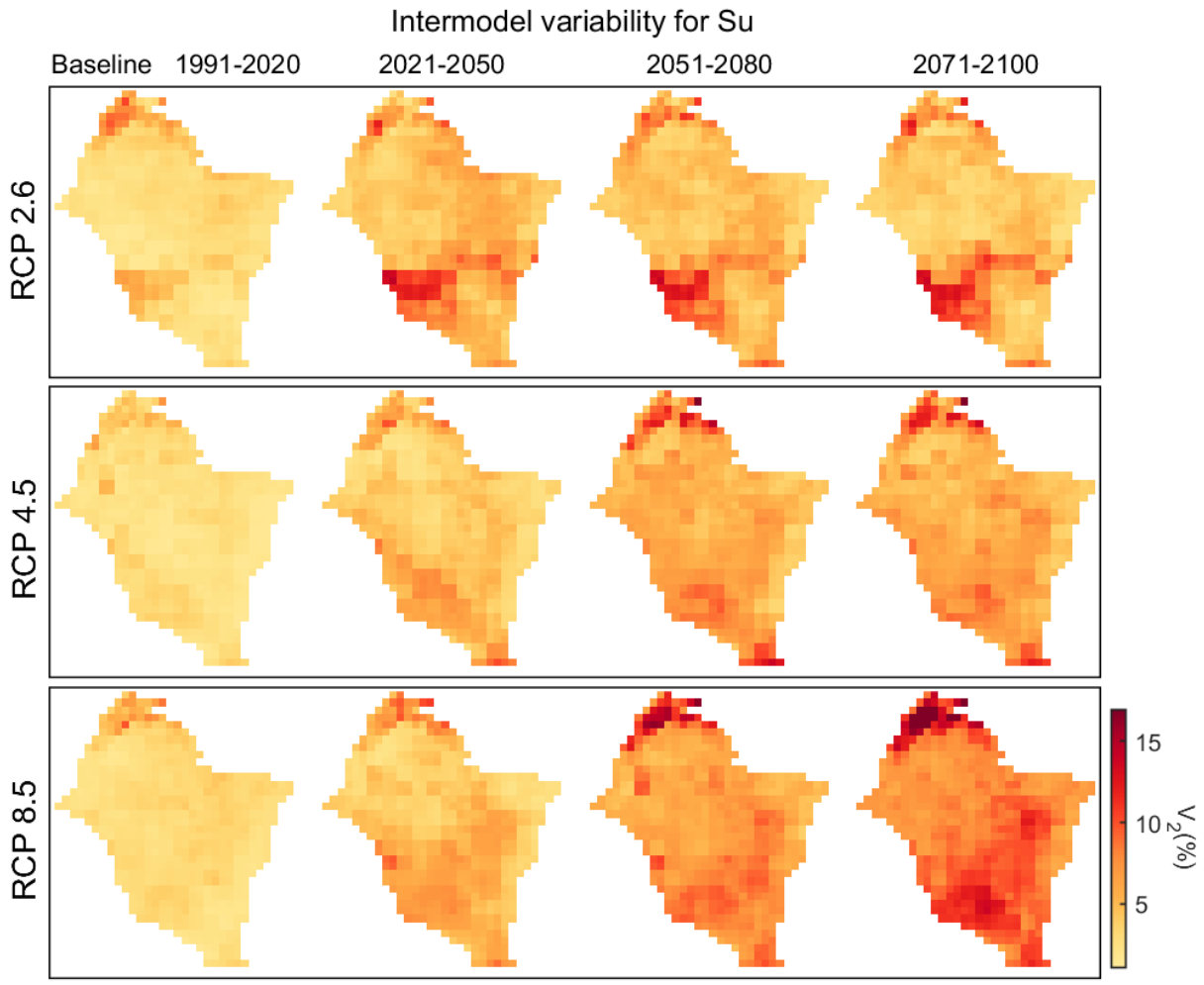

Figure S50. Spatial patterns of inter-model variability of annual root-zone soil moisture (S_u).

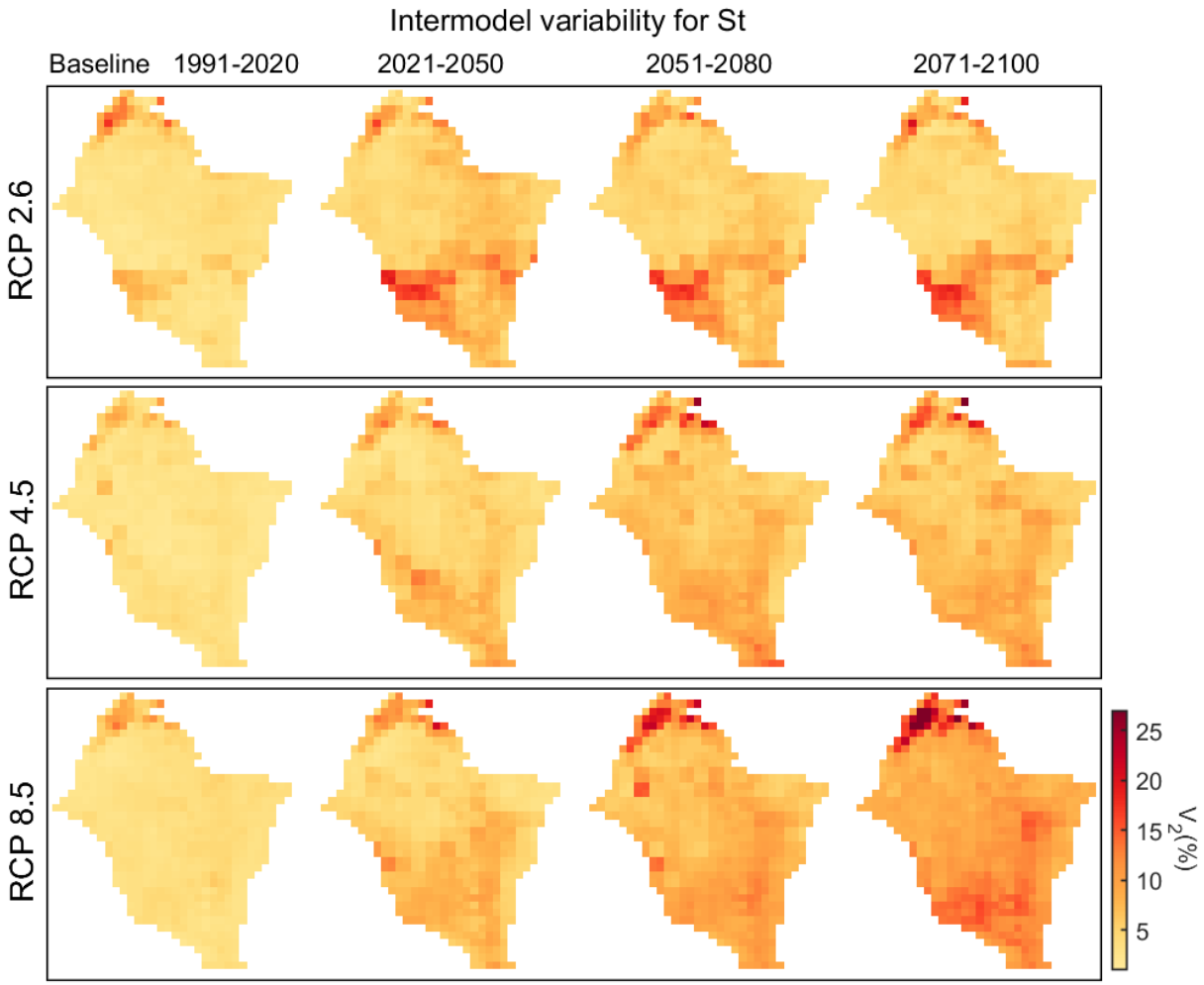

Figure S51. Spatial patterns of inter-model variability of annual terrestrial water storage (S_t).

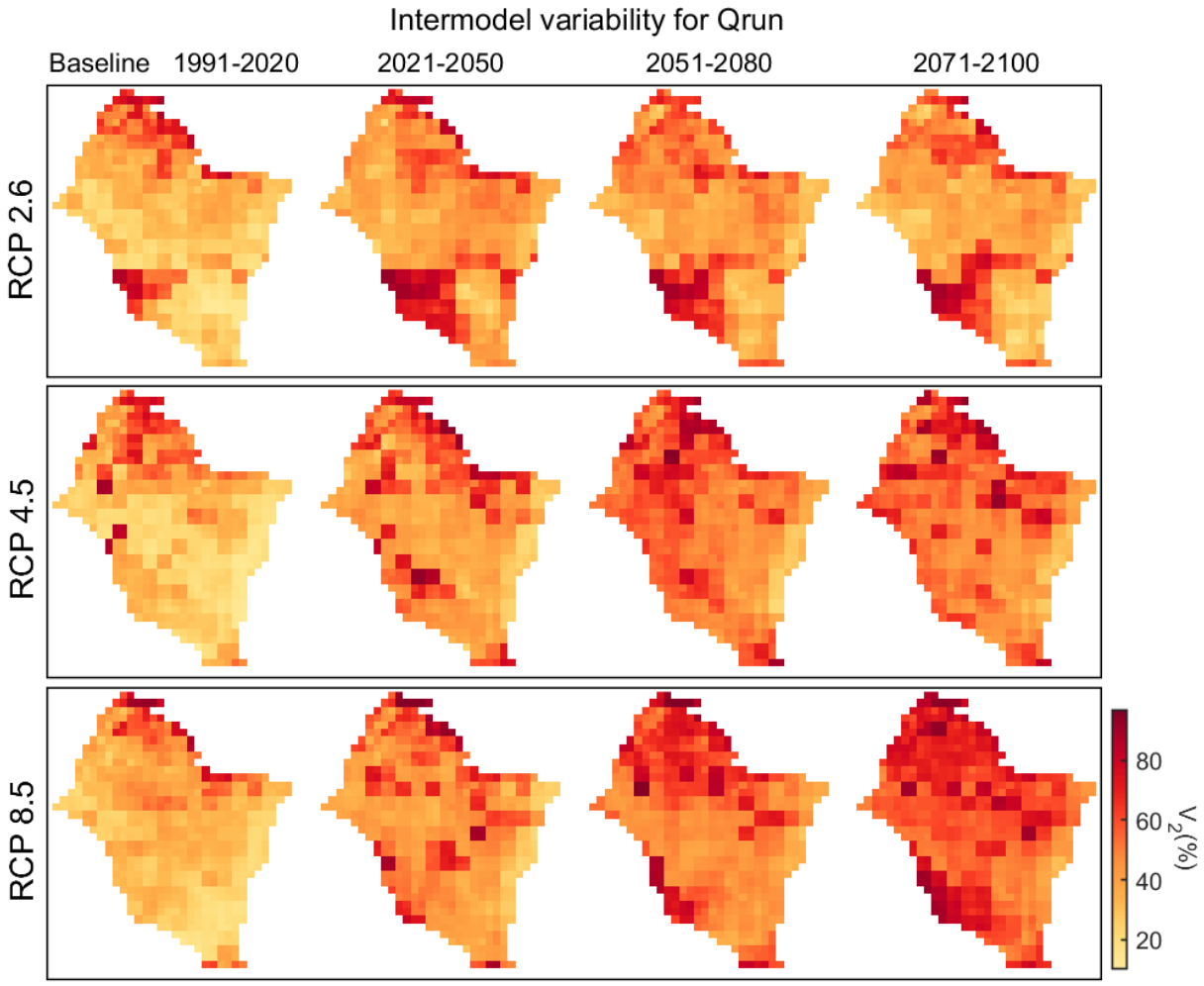

Figure S52. Spatial patterns of inter-model variability of annual total runoff (Q_{run}).

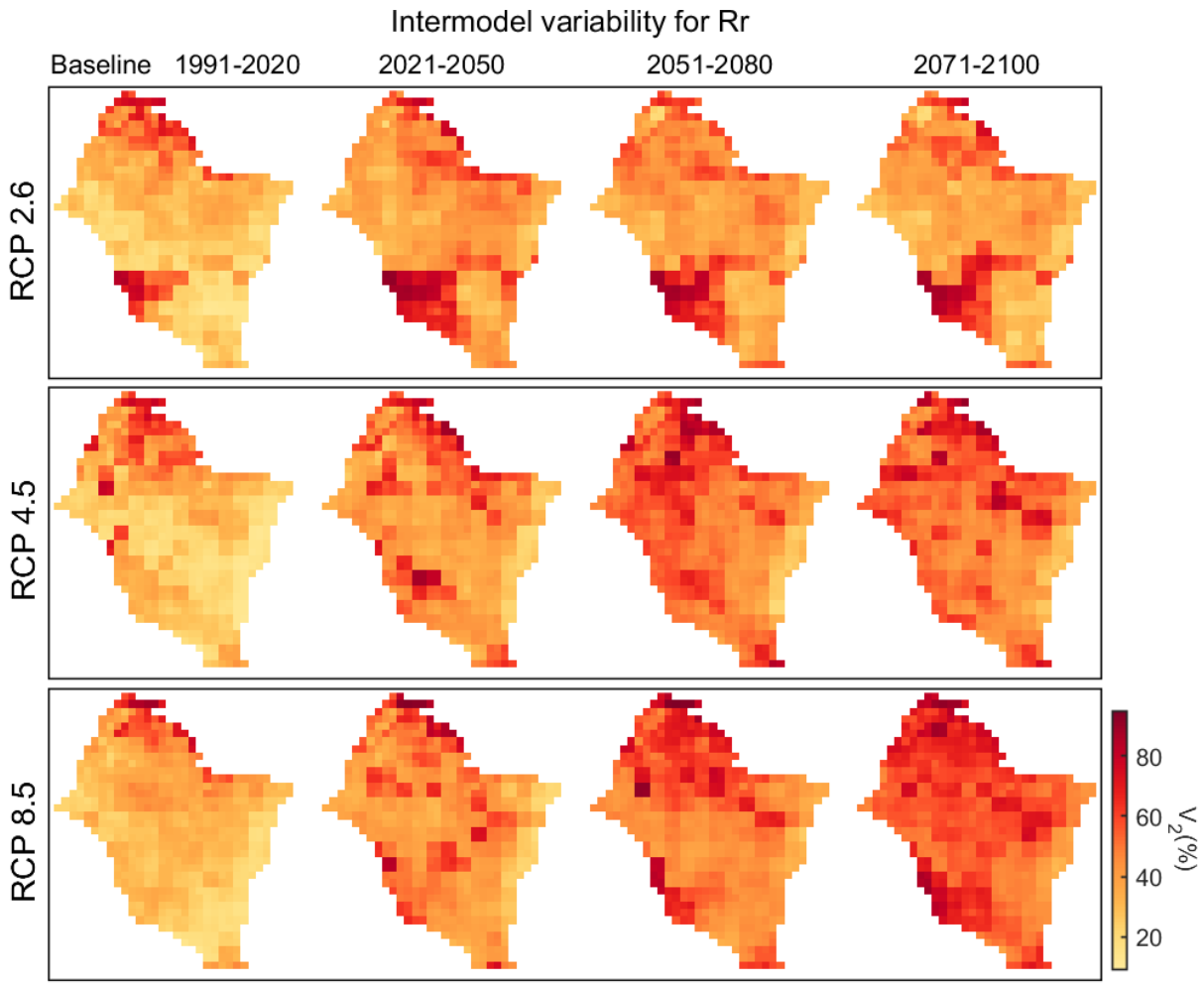

Figure S53. Spatial patterns of inter-model variability of annual groundwater recharge (R_r).

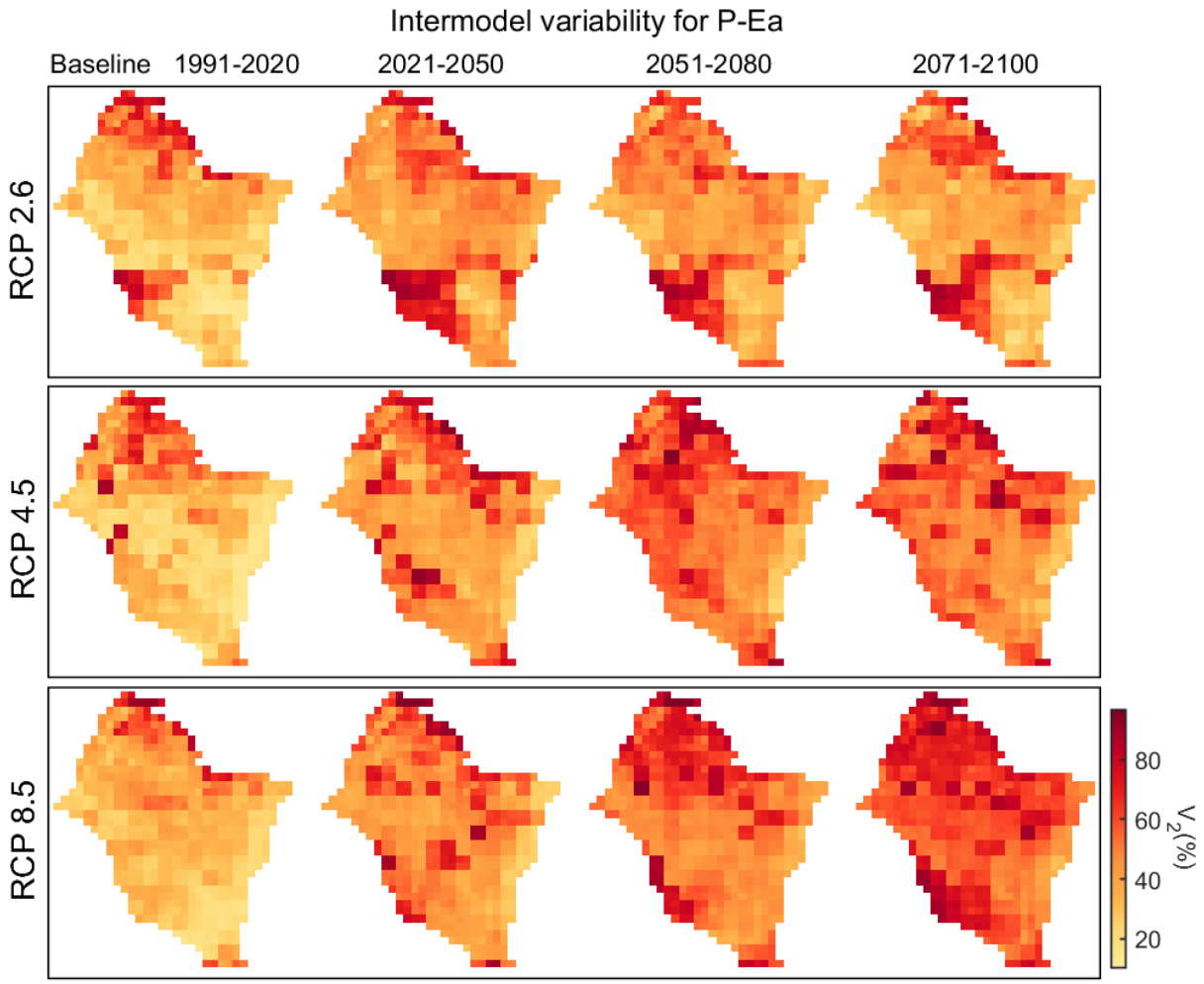

Figure S54. Spatial patterns of inter-model variability of annual water availability (P-E_a).

8 High and low flows

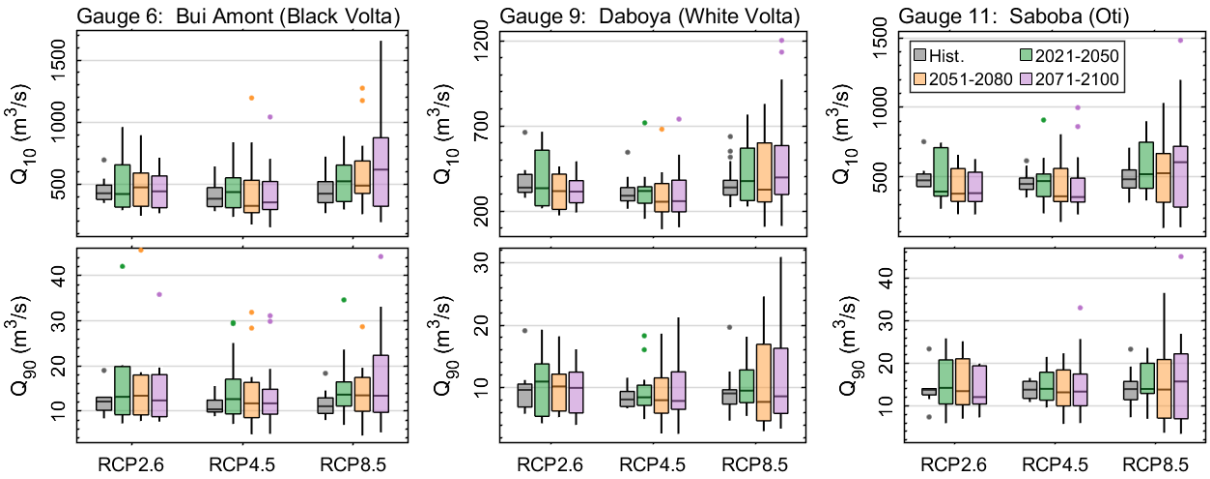

Figure S55. High flows (Q_{10}) and low flows (Q_{90}) trends over the historical (1991-2020) and future periods at selected streamflow gauges. Each boxplot represents the spread among the RCM-GCMs combinations under RCP2.6 (9 models), RCP4.5 (16 models) and RCP8.5 (18 models).

Table S1. Percentage of model agreement on the direction of change between the RCM-GCM combinations for high flows (Q_{10}) in three sub-basins (Black Volta, White Volta and Oti).

Q_{10}	**Bui Amont (Black Volta)**			**Daboya (White Volta)**			**Saboba (Oti)**		
Period	RCP2.6	RCP4.5	RCP8.5	RCP2.6	RCP4.5	RCP8.5	RCP2.6	RCP4.5	RCP8.5
2021-2050	55.6	56.3	72.2	55.6	56.3	66.7	55.6	56.3	66.7
2051-2080	55.6	62.5	66.7	66.7	56.3	55.6	55.6	75.0	55.6
2071-2100	66.7	62.5	55.6	66.7	75.0	66.7	66.7	75.0	55.6

Table S2. Percentage of model agreement on the direction of change between the RCM-GCM combinations for low flows (Q_{90}) in three sub-basins (Black Volta, White Volta and Oti).

Q_{90}	**Bui Amont (Black Volta)**			**Daboya (White Volta)**			**Saboba (Oti)**		
Period	RCP2.6	RCP4.5	RCP8.5	RCP2.6	RCP4.5	RCP8.5	RCP2.6	RCP4.5	RCP8.5
2021-2050	55.6	68.8	77.8	55.6	50.0	72.2	55.6	50.0	61.1
2051-2080	55.6	50.0	66.7	55.6	50.0	55.6	55.6	50.0	55.6
2071-2100	66.7	68.8	61.1	55.6	50.0	61.1	55.6	50.0	55.6

9 Climate sensitivity of hydroclimatic variables

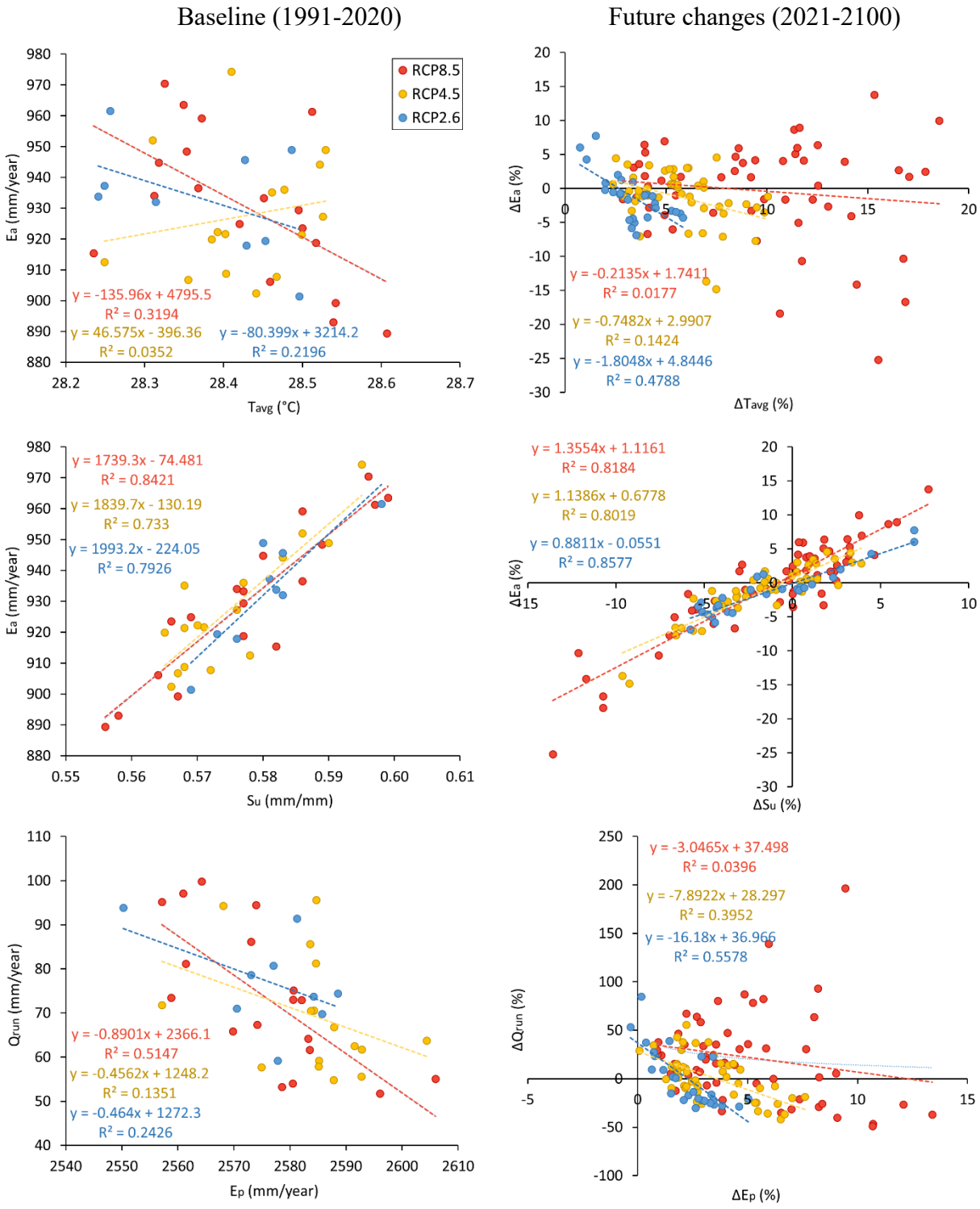

Figure S56. Climate sensitivity of hydrological processes in the VRB over the historical period (left column) with associated future changes (right column). The coloured dots represent RCM-GCM combinations per RCP and the colour dashed lines represent the fitted linear regression.

10 END